Normalization of NAD+ Redox Balance as a Therapy for Heart Failure

BACKGROUND: Impairments of mitochondrial function in the heart are linked intricately to the development of heart failure, but there is no therapy for mitochondrial dysfunction.

METHODS: We assessed the reduced/oxidized ratio of nicotinamide adenine dinucleotide (NADH/NAD+ ratio) and protein acetylation in the failing heart. Proteome and acetylome analyses were followed by docking calculation, mutagenesis, and mitochondrial calcium uptake assays to determine the functional role of specific acetylation sites. The therapeutic effects of normalizing mitochondrial protein acetylation by expanding the NAD+ pool also were tested.

RESULTS: Increased NADH/NAD+ and protein hyperacetylation, previously observed in genetic models of defective mitochondrial function, also are present in human failing hearts as well as in mouse hearts with pathologic hypertrophy. Elevation of NAD+ levels by stimulating the NAD+ salvage pathway suppressed mitochondrial protein hyperacetylation and cardiac hypertrophy, and improved cardiac function in responses to stresses. Acetylome analysis identified a subpopulation of mitochondrial proteins that was sensitive to changes in the NADH/NAD+ ratio. Hyperacetylation of mitochondrial malate-aspartate shuttle proteins impaired the transport and oxidation of cytosolic NADH in the mitochondria, resulting in altered cytosolic redox state and energy deficiency. Furthermore, acetylation of oligomycin-sensitive conferring protein at lysine-70 in adenosine triphosphate synthase complex promoted its interaction with cyclophilin D, and sensitized the opening of mitochondrial permeability transition pore. Both could be alleviated by normalizing the NAD+ redox balance either genetically or pharmacologically.

CONCLUSIONS: We show that mitochondrial protein hyperacetylation due to NAD+ redox imbalance contributes to the pathologic remodeling of the heart via 2 distinct mechanisms. Our preclinical data demonstrate a clear benefit of normalizing NADH/NAD+ imbalance in the failing hearts. These findings have a high translational potential as the pharmacologic strategy of increasing NAD+ precursors are feasible in humans.

Chi Fung Lee, PhD
Juan D. Chavez, PhD
Lorena Garcia-Menendez, DVM
Yongseon Choi, MD
Nathan D. Roe, PhD
Ying Ann Chiao, PhD
John S. Edgar, PhD
Young Ah Goo, PhD
David R. Goodlett, PhD
James E. Bruce, PhD
Rong Tian, MD, PhD

Correspondence to: Rong Tian, MD, PhD, Mitochondria and Metabolism Center, University of Washington, Room N130, 850 Republican Street, Seattle, WA 98109-8057. E-mail rongtian@u.washington.edu

Clinical Perspective

What Is New?

- We show that mitochondrial dysfunction increases NADH/NAD⁺ ratio and protein hyperacetylation resulting in a greater sensitivity of the heart to chronic stress.
- Mechanistically, we have identified that hyperacetylation of the regulators of mitochondrial permeability transition pore and malate aspartate shuttle mediates the increased susceptibility to stresses.
- Increased acetylation levels of cyclophilin D and oligomycin sensitive conferring protein on the adenosine triphosphate synthase complex promote the interaction between oligomycin sensitive conferring protein and cyclophilin D and increase mitochondrial permeability transition pore sensitivity. Moreover, hyperacetylation and inhibition of malate aspartate shuttle limits the mitochondrial import and oxidation of NADH generated in the cytosol resulting in cytosolic redox imbalance.

What are the Clinical Implications?

- The identified mechanisms described above are observed in animal models and human failing hearts.
- Our preclinical results show that expanding the cardiac NAD⁺ pool via pharmacologic or genetic approaches normalizes the NADH/NAD⁺ ratio and protein acetylation in hypertrophied and failing hearts.
- Importantly, these measures improve cardiac function and reduce pathologic hypertrophy in mice. Thus, the study identifies NADH/NAD⁺ ratio a viable therapeutic target for mitochondrial dysfunction and heart failure.

Cardiovascular disease is a leading cause of death worldwide.[1] As the life expectancy increases and the mortality of acute ischemic events decreases, the incidence of heart failure is mounting at a pace of 900 000 per year.[2] However, medical therapy for heart failure has been stalled for almost 2 decades. Novel concepts and strategies in the treatment of heart failure are needed urgently.

The heart is a high energy-consuming organ. Mitochondrion is the powerhouse of the cell and mitochondrial dysfunction is a well-recognized maladaptive mechanism during the development of heart failure.[3,4] Targeting mitochondria for heart failure therapy has long been sought; however, previous work focusing on improving mitochondrial energy production and reducing reactive oxygen species yielded few successful clinical applications.[5] In recent years, protein lysine acetylation emerged as an important mechanism linking mitochondrial metabolism to cellular pathologies.[6–8] The level of protein acetylation reflects the balance of acetylation and deacetylation. Although the former is dependent on the abundance of acetyl-CoA and the activity of acetyl-

transferase, the later is determined by the deacetylase activity, and primarily sirtuins in the mitochondria. The sirtuin deacetylases consume NAD⁺ as a cosubstrate[9]; mitochondrial function is critical for setting the NADH/NAD⁺ balance thus the NAD⁺ available for sirtuin activity.

Using a mouse model with primary mitochondrial dysfunction (cardiac-specific deletion of a Complex-I protein, Ndufs4: cKO), we recently found that elevation in NADH/NAD⁺ ratio induce mitochondrial protein hyperacetylation and renders the heart highly susceptible to stresses.[10] In this study we defined the molecular intermediaries linking specific NAD⁺-sensitive hyperacetylation targets to the development of heart failure and demonstrated the relevance of these mechanisms in human heart failure. Furthermore, we showed that restoring the NADH/NAD⁺ ratio by genetic and pharmacologic approaches is an effective and potentially translatable strategy for the treatment of heart failure in clinical practice.

METHODS

Animal Care, Surgical Procedures, and Echocardiography

All procedures involving animal use were performed with the approval of Institutional Animal Care and Use Committee of the University of Washington. Procedures for animal care, surgeries, and echocardiography were in the online-only Data Supplement.

Ex Vivo Measurements of Cardiac Function and Energetics

Langendorff perfused mouse hearts were isolated as described in the online-only Data Supplement.[11]

Mitochondrial Isolation, Proteome, and Acetylome Analyses

Mitochondria were isolated as described.[12] Peptide generation and mass spectrometric protocols were in the online-only Data Supplement.

Acquired tandem mass spectra were searched for sequence matches against the International Protein Index mouse database using SEQUEST. The following modifications were set as search parameters: peptide mass tolerance at 500 ppm, trypsin digestion cleavage after K or R (except when followed by P), one allowed missed cleavage site, carboxymethylated cysteines (static modification), and oxidized methionines or acetylation on K (variable modification). PeptideProphet[13] and ProteinProphet[14] were used to assign confidence in the identified spectra resulting from the SEQUEST search. It relies on probability models and an empirical Bayesian approach to model fitting. First a score is produced to reflect the quality of each spectrum. Then a probability-based model is produced for the distribution of correctly and incorrectly identified spectra and fit to the scores of all identified spectra. The confidence in individual spectra are evaluated using the posterior probability. A cutoff is applied on the scores for the set of correctly identified spectra to control the false discovery rate, defined as the percentage of

false positives which pass the cutoff. This method produces a similar estimation of the false discovery rate as the commonly used target-decoy search strategy.[15] For more details on the statistics used in the Prophets we refer readers to Ma et al.[16] We used a PeptideProphet probability ≥0.9 and ProteinProphet probability ≥0.9 for positive identification at an error rate of >1%. Differences in relative expression of proteins were calculated using peptide spectral counting algorithm.[17]

Comet (v2013.02 rev1)[18] was used to search the mass spectral data against the UniProt protein database for *Mus musculus* containing forward and reverse sequences (33 224 total protein sequences). Comet search parameters included a precursor mass tolerance of 25 ppm, allowing for up to 3 13C offset. Trypsin was selected as the digesting enzyme allowing for up to 2 missed cleavage sites. Variable modifications included oxidation of Met (15.9949 Da) and acetylation on Lys or protein n-termini (42.010565 Da). Static modifications included carbamidomethylation of Cys (57.021464 Da). Fragment ion mass tolerance was set to 0.02 Da. Resulting peptide spectrum matches were filtered to <1% false discovery rate using a forward/reverse sequence strategy.

Molecular Docking Calculation

Detailed methods of molecular docking of cyclophilin D (CypD) and oligomycin-sensitive conferring protein (OSCP) were in the online-only Data Supplement.

Mitochondrial Calcium Uptake Assay and Biochemical Assays

Methods of mitochondrial calcium uptake assays and all biochemical assays used in this study were in the online-only Data Supplement.

Antibodies, Western Blot, and Immunoprecipitation

Methods of antibodies, Western blot, and immunoprecipitation were in the online-only Data Supplement.

Statistical Analysis

Comparisons among the multiple groups were performed by 1-way analysis of variance, followed by Newman-Keuls multiple comparison test. For comparisons only involving 2 groups, unpaired 2-tailed t-tests were used. For repeated measurements of multiple groups, 2-way repeated measure analysis of variance was performed. All analyses were performed using GraphPad Prism 6.0. All data are expressed as mean±SEM and a $P<0.05$ was considered significant. All analyses were validated with permutation test versions, which are not dependent on any assumption of data distribution.[19]

RESULTS

Protein Hyperacetylation in the Failing Heart Was Reversed by Expanding the NAD+ Pool

We showed previously that increased NADH/NAD+ ratio and inhibition of NAD+- dependent protein deacetylation

caused by mitochondrial Complex-I deficiency (cKO) increased cardiac susceptibility to stress.[10] We sought to test whether protein hyperacetylation occurs during the development of heart failure. In cardiac tissues of patients with heart failure with ischemic or dilated cardiomyopathy (online-only Data Supplement Table I), we observed higher acetylation levels compared with nonfailing human hearts (Figure 1A). In addition, pressure overload generated by transverse aortic constriction (TAC) elevated cardiac NADH/NAD+ ratio and mitochondrial protein hyperacetylation (Figure 1B-C, Figure IA-B in the online-only Data Supplement), further supporting a positive correlation of NAD+-sensitive protein acetylation and heart failure development. Next, we tested whether restoring NADH/NAD+ balance by either a genetic or pharmacologic approach can normalize protein acetylation. We elevated NAD+ synthesis via the NAD+ salvage pathway by supplementing NAD+ precursor nicotinamide mononucleotide (NMN) or overexpressing the rate-limiting enzyme, nicotinamide phosphoribosyltransferase, in the mouse hearts (cNAMPT, Figure 1D; Figure IC in the online-only Data Supplement).[20] Both measures increased NAD+ level[10,20] without affecting cardiac function in unstressed mice (Figure ID-H in the online-only Data Supplement). NMN administration normalized the NADH/NAD+ ratio and importantly, reversed mitochondrial protein hyperacetylation in control mice after TAC (Figure 1B-C, Figure IA-B in the online-only Data Supplement). Similarly, NMN administration also attenuated the NAD+ redox imbalance and protein hyperacetylation induced by primary mitochondrial dysfunction in cKO hearts (Figure 1E-F, Figure II-J in the online-only Data Supplement). The data from multiple models collectively indicate that the NAD+-dependent protein hyperacetylation is present in failing hearts and hearts with mitochondrial dysfunction, which can be abrogated by elevation of NAD+ levels and restoration of the NADH/NAD+ balance.

Normalization of Protein Acetylation Blunted the Development of Heart Failure During Chronic Stresses

Next, we sought to determine if the reversal of protein hyperacetylation by NMN would improve cardiac function and reduce pathologic hypertrophy induced by pressure overload. TAC caused significant cardiac hypertrophy, left ventricular dilation and decline in fractional shortening in control mice (Figure 2A-D, Figure IIA in the online-only Data Supplement). NMN administration improved fractional shortening (Figure 2A), left ventricular dilation and hypertrophy (Figure 2B-D) in TAC-stressed mice. In addition, the accelerated course of heart failure in cKO mice after TAC (Figure IIB in the online-only Data Supplement)[10] also was abrogated by NMN administration. NMN treatment preserved contractile function (Figure 2E), reduced cardiac hypertrophy, left ventricular dilation, and
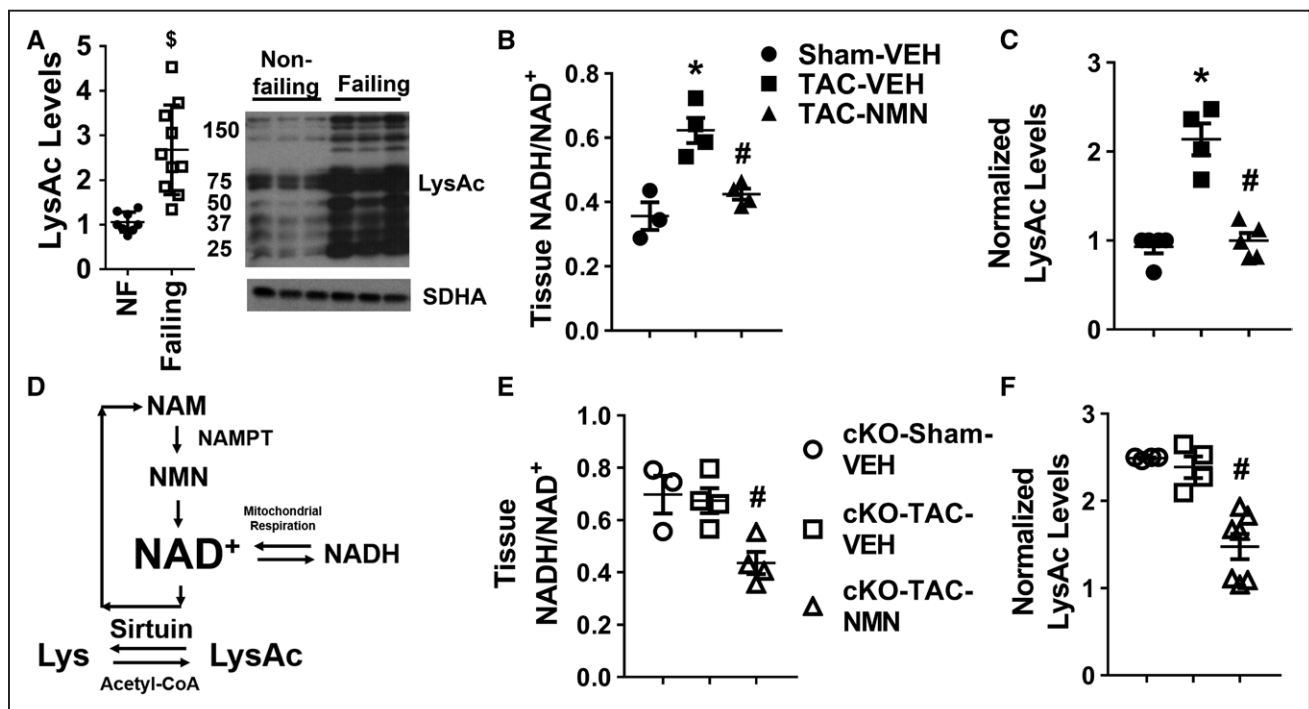
Figure 1. Protein hyperacetylation in the failing hearts was normalized by restoring the NADH/NAD+ ratio.
A, Acetylation of human failing hearts were estimated by Western blotting. N=8 to 10. The ratio of heart failure patients with ischemic versus dilated cardiomyopathy is 1:1. **B,** Tissue NADH/NAD+ ratio and **(C)** mitochondrial protein acetylation levels by Western blotting of control mice 4 weeks after sham or transverse aortic constriction (TAC) surgeries with and without nicotinamide mononucleotide (NMN) treatment were measured. N=3 to 4. **D,** Sirtuin deacetylase reaction requires NAD+. Mitochondrial NAD+ level is determined by the NADH/NAD+ ratio and the rate of NAD+ synthesis via salvage pathway. Nicotinamide phosphoribosyltransferase (NAMPT), the rate limiting enzyme of this pathway, catalyzes the conversion of nicotinamide (NAM) into NMN. Overexpression of NAMPT and supplementation of NMN were used to elevate NAD+ levels in this study. **E,** Tissue NADH/NAD+ ratio and **(F)** mitochondrial protein acetylation in cardiac tissues of the cKO mice were measured. N=3 to 4. *$P<0.05$ compared with sham-vehicle; #$P<0.05$ compared with TAC-VEH; and $$P<0.05$ compared with nonfailing. All data are expressed as means ±SEM.

lung edema (Figure 2F-H, Figure IIC-D in the online-only Data Supplement). The data strongly supported the efficacy of NMN administration in delaying the development of heart failure in mice with mitochondrial dysfunction, either primary or acquired.

We also tested whether elevation of NAD+ levels specifically in heart by increasing NAMPT activity also would be effective to prevent cardiac dysfunction and hypertrophy induced by another stressor with distinct mechanism, isoproterenol (ISO) stimulation. Transgenic mice overexpressing NAMPT only in the hearts (cNAMPT)[20] were crossed with control and cKO mice to obtain mice with cNAMPT expression. We stressed the mice by chronic β-adrenergic stimulation with isoproterenol, which has been shown to cause cardiac myocyte death and pathologic hypertrophy.[21] Isoproterenol (30 mg/kg/d) delivered by osmotic minipump for 2 weeks (Figure IIIA in the online-only Data Supplement) induced significant cardiac dysfunction and hypertrophy in both control (Figure 3A-D, Figure IIIB in the online-only Data Supplement) and cKO mice (Figure 3E-H, Figure IIIC in the online-only Data Supplement) while cKO mice pre-

sented worse phenotypes. Elevation of cardiac NAD+ levels by cNAMPT protected both mice from isoproterenol-induced cardiac dysfunction, LV dilation, and hypertrophy (Figure 3, Figure III in the online-only Data Supplement). The data also supported that targeting the NAD+ salvage pathway to elevate cellular NAD+ levels represents a viable intervention strategy to improve cardiac function in response to chronic stresses. Moreover, the cNAMPT mice provide a useful tool to dissect the mechanistic roles of NADH/NAD+- sensitive protein acetylation in heart failure propensity.

Acetylome Analyses Identified NADH/NAD+-Sensitive Changes in Acetylation Landscape

To test the hypothesis that protein acetylation that is sensitive to NADH/NAD+ ratio modulates cardiac sensitivity to stress, we performed acetylome analysis of cKO hearts with and without cNAMPT. We first compared the mitochondrial proteomes from control and cKO hearts to rule out the possibility that increases in acetylated proteins in cKO were due to increases in the total pro-
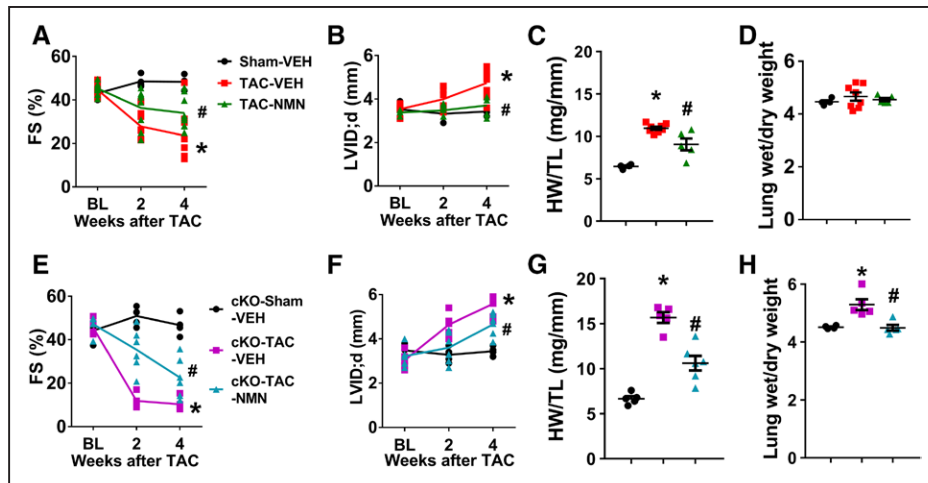
Figure 2. Nicotinamide mononucleotide (NMN) protected hearts from pathologic hypertrophy and contractile dysfunction induced by chronic pressure overload.

A, Fractional shortening (FS), **(B)** left ventricular (LV) dilation (left ventricular internal dimension at diastole [LVID;d]), **(C)** cardiac hypertrophy (heart weight/tibia length, [HW/TL] at 4-week end point), and **(D)** lung edema (wet/dry lung weight at 4-week end point) of control mice after sham or transverse aortic constriction (TAC) surgeries with or without NMN treatment were assessed. N=5 to 8. **E,** FS, **(F)** LV dilation, **(G)** cardiac hypertrophy, and **(H)** lung edema of cKO mice after indicated treatments were assessed. N=5 to 6. *$P<0.05$ compared with corresponding sham; and #$P<0.05$ compared with corresponding TAC-vehicle. All data are expressed as means±SEM.

tein amount. We did not observe significant up-regulation of mitochondrial protein levels while multiple proteins in mitochondrial complex-I were downregulated (Table II-III and Figure IVA-B in the online-only Data Supplement). This is consistent with the observation that deletion of Ndusf4 resulted in poor assembly of complex-I and hence degradation of complex-I proteins.[10] Despite the minimal changes in protein levels, the number of acety-

lated proteins (Figure 4A) and acetylation levels of peptides increased in cKO hearts (Figure 4B), consistent with increased acetylation shown by Western blot (Figure 4C, Figure IVC in the online-only Data Supplement). Hyperacetylation of some known protein targets were validated by Western blots (Figure IVD-E in the online-only Data Supplement). Increased acetylation levels in cKO hearts were not attributable to alterations in the levels of
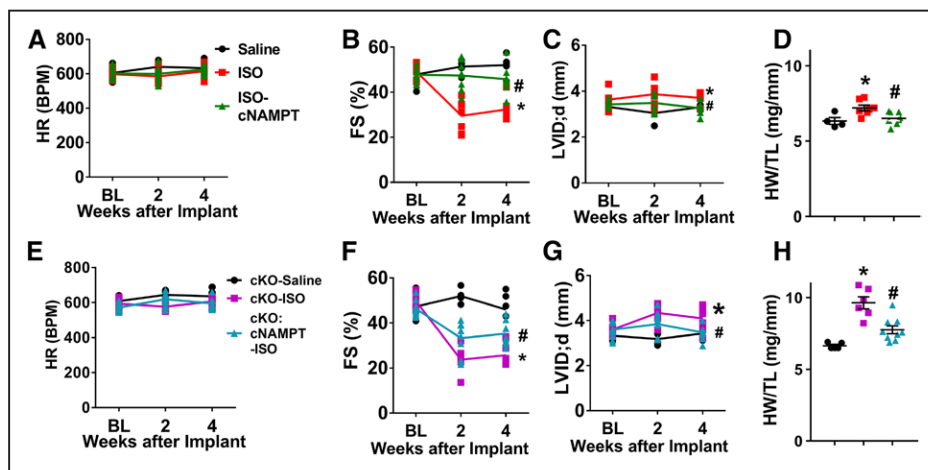
Figure 3. Cardiac nicotinamide phosphoribosyltransferase (NAMPT) expression reversed isoproterenol- (ISO) induced cardiac dysfunction and hypertrophy.

A, Heart rate (HR), **(B)** fractional shortening (FS), and **(C)** left ventricular internal dimension at diastole (LVID; d), and **(D)** cardiac hypertrophy (heart weight/tibia length [HW/TL]) of control or control+cNAMPT mice challenged with saline or isoproterenol (ISO, 30 mg/kg/d) for 2 weeks were measured. N=5 to 9. **E,** HR, **(F)** FS, **(G)** LVID; d, ratio of **(H)** HW/TL of complex-I protein (cKO) or cKO+cNAMPT mice challenged with saline or ISO were recorded. N=5 to 8. *$P<0.05$ compared with corresponding saline; #$P<0.05$ compared with corresponding ISO. Data are expressed as means±SEM.
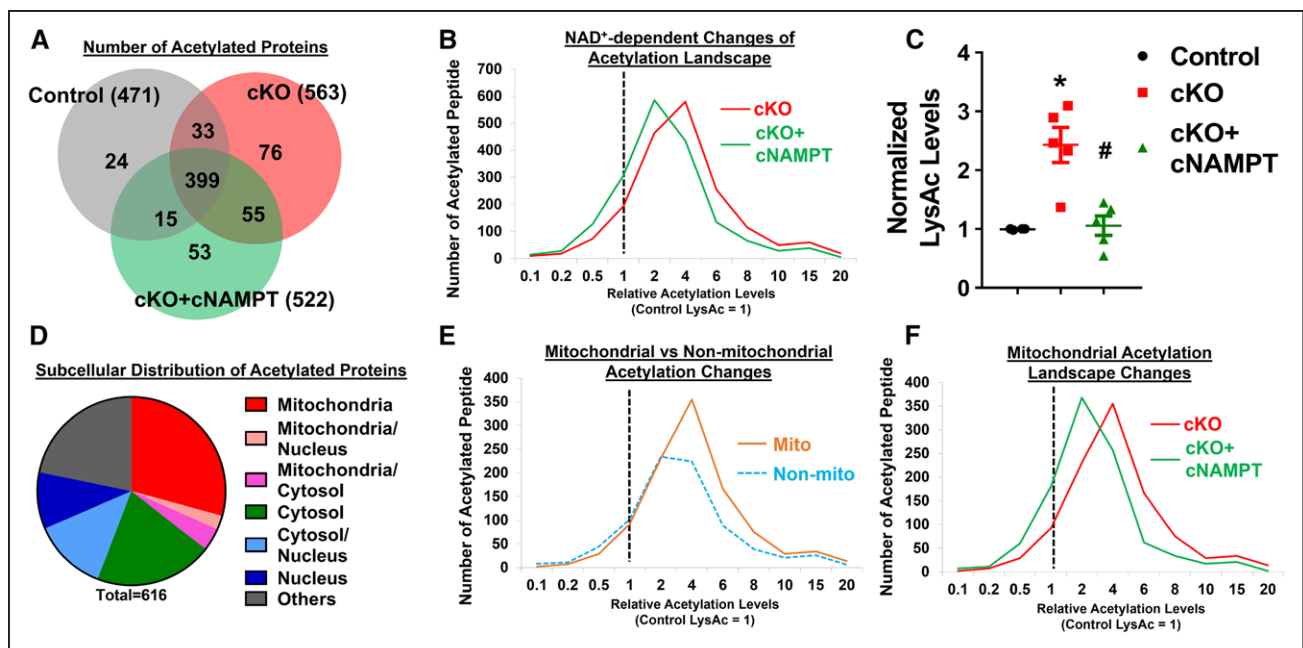
Figure 4. Acetylome analysis identified NADH/NAD+-sensitive changes in acetylation landscape.
A, Venn diagram showing the overlapping of acetylated proteins identified in control, complex-I protein (cKO), and cKO+cNAMPT hearts. Numbers in bracket represent the total number of acetylated proteins identified in each group. B, Acetylated peptides of cKO and cKO+cNAMPT hearts were quantified by liquid chromatography–mass spectrometry and normalized to control values. Distribution of the acetylation changes was plotted. Dotted line at 1 was set to the mean of control peptide levels. Distribution shift to the right of 1 represented increased acetylation levels compared to control. C, Acetylation levels from indicated hearts were assessed by Western blot. *P<0.05 compared with control. #P<0.05 compared with cKO. D, Pie chart showing subcellular localization of acetylation proteins identified in cKO hearts. E, Changes of acetylation in mitochondrial (mito) versus nonmitochondrial (nonmito) compartments. F, Mitochondrial acetylation landscape changes of cKO and cKO+cNAMPT hearts were compared.

acetyl-CoA, mitochondrial acetyltransferase GCN5L1, or sirtuin expressions (Figure IVF-G in the online-only Data Supplement). As expected, cNAMPT overexpression normalized the NADH/NAD+ ratio and hyperacetylation in cKO hearts (Figure 4C, Figure IVC, H in the online-only Data Supplement). The number of acetylation proteins as well as the levels of acetylated peptides in cKO hearts were reduced by cNAMPT (Figure 4A-B, left-shift from cKO). Although mitochondrial proteins only constituted about a third of the 616 acetylated proteins identified (Figure 4D), a disproportionately high fraction of hyperacetylated peptides were originated from mitochondrial proteins in cKO (Figure 4E), and they responded robustly to the normalization of NADH/NAD+ ratio by cNAMPT (Figure 4F, left-shift from cKO). These observations also support a critical role of NADH/NAD+ ratio in connecting mitochondrial function and acetylation landscape. Interestingly, acetylation levels of proteins from nonmitochondrial compartments also were elevated in cKO hearts (Figure 4E, right-shift from 1). Expression of cNAMPT moderately reduced the acetylation of nonmitochondrial proteins (Figure IVI in the online-only Data Supplement). This observation raised an intriguing possibility that the NAD+ redox imbalance caused by mitochondrial dysfunction could affect other cellular compartments, and as such contributed to pathologic remodeling of the heart

by altering cytosolic redox state and whole cell hyperacetylation.

Acetylation of Malate Aspartate Shuttle Regulated Cytosolic NAD+ Redox Balance and Cardiac Energetics

Among the subpopulation of proteins whose acetylation responded robustly to NADH/NAD+ ratio, hyperacetylation of the mitochondrial isoforms of malate aspartate shuttle (MAS) proteins (Figure 5A, Table IV in the online-only Data Supplement) is of interest. MAS is a key player in the communication of cytosolic and mitochondrial NAD+ redox states,[22] carrying electrons from cytosolic NADH into mitochondria for oxidative phosphorylation.[23] Decreased MAS activity was found in cKO and isoproterenol-treated hypertrophic hearts, and in both cases could be restored by overexpressing cNAMPT (Figure 5B-C). Acetylation of a number of lysines in the MAS proteins was reduced toward normal level by overexpressing cNAMPT (Table IV in the online-only Data Supplement). Moreover, incubation of mitochondrial proteins with acetyl-coA promoted acetylation of mitochondrial GOT2 (glutamate oxaloacetate transaminase) and inhibited its activity (Figure VA-C in the online-only Data Supplement), also supporting the notion that protein hyperacetylation
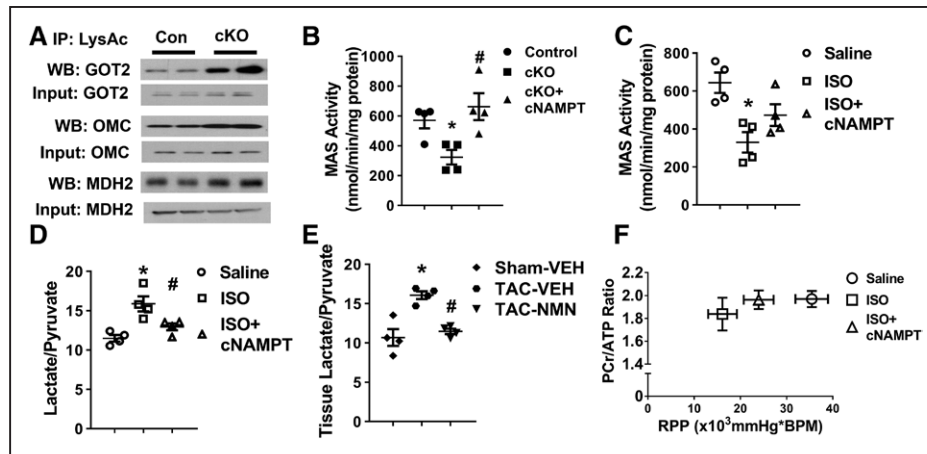
Figure 5. Inhibition of malate aspartate shuttle (MAS) by acetylation altered cytosolic redox state and cardiac energetics.

A, Acetylation levels of mitochondrial isoforms of MAS proteins were assessed by immunoprecipitation/Western blot (IP-WB) analysis. N=4. MAS activity of mitochondria isolated from **(B)** control, cKO and cKO⁺cNAMPT and **(C)** isoproterenol- (ISO) treated hearts were measured. N=4. Tissue lactate/pyruvate ratio of **(D)** ISO-treated or **(E)** transverse aortic constriction- (TAC) stressed hearts were measured. N=4. **F,** The relationship between cardiac energetics, estimated by phosphocreatine to adenosine triphosphate ratio (PCr/ATP) and contractile function, estimated by rate pressure product (RPP), measured simultaneously in isolated perfused hearts by ³¹P NMR spectroscopy. N=4. *$P<0.05$ compared with corresponding control/saline/sham-vehicle; and #$P<0.05$ compared with corresponding cKO/ISO/TAC-VEH. All data are expressed as means±SEM.

suppressed the shuttle activity. The lactate/pyruvate ratio, a marker for cytosolic NADH/NAD⁺ ratio, was elevated in isoproterenol-treated and TAC-stressed hearts and was lowered by cNAMPT or NMN (Figure 5D-E). The data collectively suggest that hyperacetylation of MAS decreases the import of cytosolic NADH into mitochondria for oxidation hence altered cytosolic NADH/NAD⁺ ratio.

Upregulation of glycolysis is a hallmark of metabolic remodeling in pathologic hypertrophy.[24,25] Elevation of MAS flux under these conditions would facilitate aerobic glycolysis for adenosine triphosphate (ATP) production.[24–28] It was shown previously that elevated MAS flux at early stage of pathological hypertrophy was attenuated as the heart transitions into energetic and contractile failure, even though the MAS protein levels were unaltered.[28] To test whether inhibition of MAS by acetylation is partially responsible for the impaired energetics in pathologic hypertrophy, we performed ³¹P NMR (31 phosphorus nuclear magnetic resonance) spectroscopy of isolated perfused hearts to measure myocardial high energy phosphate content and contractile function simultaneously. We observed a downward-left shift in the relationship of myocardial energetic status assessed by phosphocreatine to ATP ratio (PCr/ATP) and contractile function assessed by the rate pressure product in isoproterenol-treated hearts (Figure 5F). The impairments were improved by partially restored MAS activity via overexpressing cNAMPT (Figure 5C, F, upward-right shift in plot). These results suggest that acetylation of MAS proteins is a key mechanism through which mitochon-

drial dysfunction impacts energetics via redox-sensitive regulations during pathological remodeling.

Acetylation of OSCP and CypD Increased mPTP Sensitivity in the Failing Heart

We previously showed that increased cardiac susceptibility to stresses in cKO hearts partly is attributable to the hypersensitivity of calcium-triggered mitochondrial permeability transition pore (mPTP) opening 10. Here we found that similar to cKO, mitochondria isolated from TAC hearts demonstrated a lower calcium retention capacity, indicating increased sensitivity of mPTP opening, which were normalized by elevation of NAD⁺ levels (Figure 6A, Figure VIA in the online-only Data Supplement). Several hyperacetylated proteins identified by acetylome analysis participate in mPTP regulation (Table V in the online-only Data Supplement) such as CypD and OSCP, and the majority of the hyperacetylated sites on these proteins were responsive to NADH/NAD⁺ ratio (Table V in the online-only Data Supplement). Although the physical identity of the mPTP remains elusive, CypD is an undisputed regulator of the mPTP.[29,30] Recent studies suggest that mitochondrial ATP synthase forms the mPTP 31, and the opening of mPTP is regulated through the interaction of CypD with OSCP subunit of ATP synthase.[31,32] We observed increased acetylation of both CypD and OSCP in cKO mitochondria and in human failing hearts (Figure 6B-C and Figure VIB, Table V in the online-only Data Supplement). Furthermore, increased acetylation was associated with increased interaction of OSCP-CypD

ORIGINAL RESEARCH ARTICLE
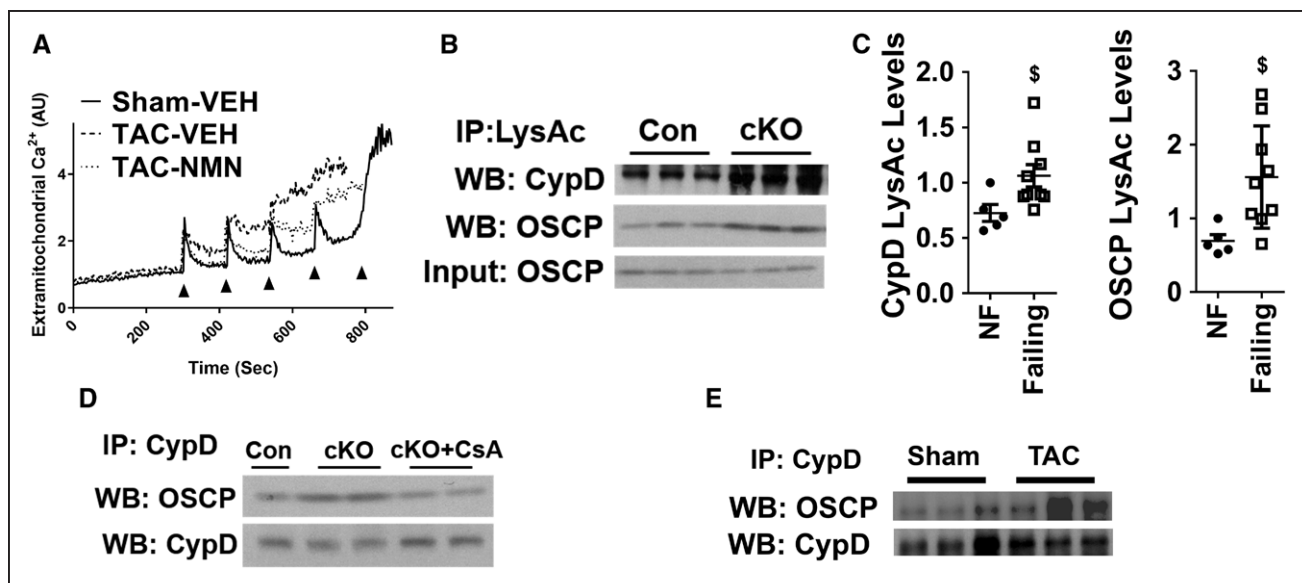
Figure 6. Acetylation promoted the interaction between oligomycin-sensitive conferring protein (OSCP) and cyclophilin D (CypD) and increased the sensitivity of mitochondrial permeability transition pore (mPTP).
A, Representative experiment of calcium-stimulated mPTP opening in mitochondria isolated from sham or transverse aortic constriction (TAC) hearts with and without nicotinamide mononucleotide (NMN) treatment. N=3 to 4. Arrows represent each calcium pulse. **B,** Acetylation levels of CypD and OSCP in control (Con) and cKO mitochondria determined by immunoprecipitation/Western blot (IP-WB). N=3. **C,** Acetylation levels of CypD and OSCP from nonfailing and failing human hearts were quantified. N=5 to 9. $P<0.05 compared with nonfailing. **D,** Interaction of CypD with OSCP were determined by IP-WB in mitochondria isolated from cKO hearts. N=3 to 4. Cyclosporine A (CsA) was added to mitochondria at a final concentration of 1 μmol/L. **E,** Interaction of CypD with OSCP in heart tissues after sham/TAC surgeries was assessed by IP-WB.

in cKO, TAC-stressed, or isoproterenol- treated hearts (Figure 6D-E, Figure VIC in the online-only Data Supplement). The increased interaction of OSCP-CypD in cKO was alleviated by cyclosporine A, an established mPTP inhibitor (CsA; Figure 6D), indicating the importance of such an interaction in regulating mPTP sensitivity. The data strongly suggest that NAD+-sensitive acetylation modulates the OSCP-CypD interaction and thus the mPTP sensitivity in hearts with pathologic hypertrophy.

Acetylation of OSCP-K70 Promoted OSCP-CypD Interaction and the mPTP Opening

To identify specific acetylation sites on OSCP and CypD responsible for regulating the protein-protein interaction, crystal structures of CypD[33] and OSCP of ATP synthase[34] were subjected to molecular docking.[35] Docking results from the highest scoring solutions consistently identified an interaction interface of OSCP with variable CypD orientations (Figure VIIA in the online-only Data Supplement). The conserved interface coincided with an empty space next to OSCP in F_1-ATP synthase, which serves as a potential interaction interface for CypD binding on the intact F_1-ATP complex (Figure VIIA-C in the online-only Data Supplement). Acetylated lysine residues identified in the 2 proteins from the acetylome analysis were mapped to the docked models (Figure 7A, left panel magenta spheres, Table V in the online-only Data Supplement).

Analysis of the top-10 scoring docking solutions revealed that OSCP-K70 always was present in the putative interaction interface. Acetylation of OSCP-K70 (OSCP-K70Ac) was normalized by cNAMPT expression in cKO (Table V in the online-only Data Supplement). In addition, OSCP-K70 is highly conserved among species surveyed (Figure VIID in the online-only Data Supplement, red asterisk) while other lysines (16 out of 21 lysines) are not. Seven out of the top-10 docking solutions showed that several different lysine residues of CypD could be in close contact with OSCP-K70 (data not shown). In 2 of these solutions, OSCP-K70 was in close proximity (3.1 Å) of CypD-K66, which would result in charge repulsion, destabilizing the OSCP-CypD interaction (Figure 7A, right panel, magenta sticks). Previous studies suggest that hyperacetylation of CypD-K166 modulate mPTP sensitivity.[36,37] Although CypD- K166Ac was not detected in our acetylome analysis (Table V in the online-only Data Supplement), it was one of the lysines from CypD found within the interaction interface out of the highest scoring docking solutions. This suggests that CypD-K166 may cause repulsion with OSCP-K70 and regulate mPTP opening.

Electrostatic interaction was suggested in regulating the OSCP-CypD interaction.[31] Together with the structural information (Figure 7A, Figure VIIA-C in the online-only Data Supplement), we hypothesized that OSCP-K70Ac promotes the OSCP-CypD interaction and sensitizes mPTP opening by alleviating electrostatic repulsion. To
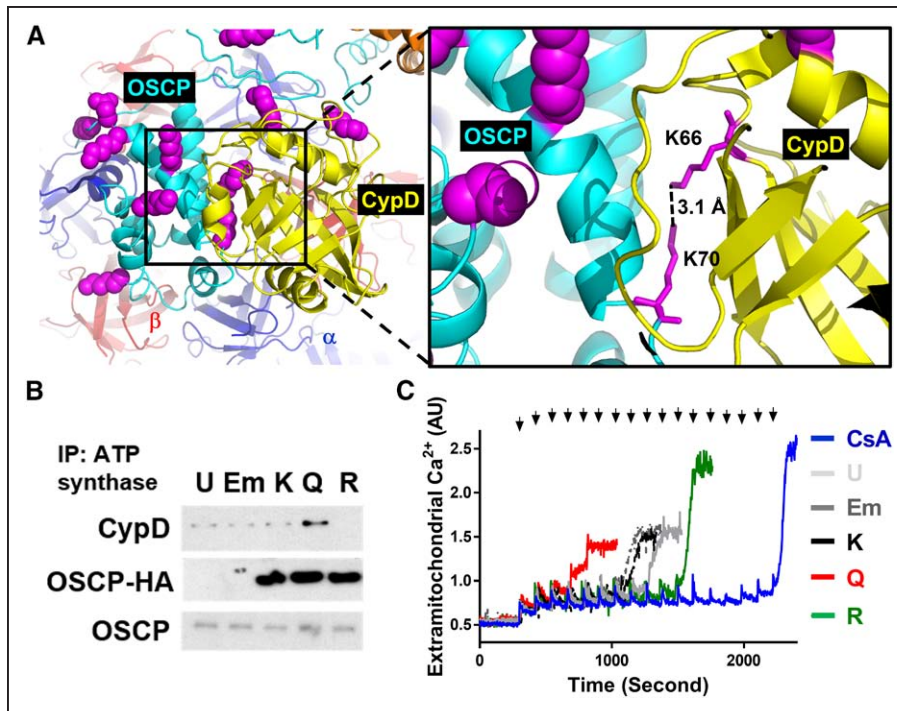
Figure 7. Acetylation of oligomycin-sensitive conferring protein- (OSCP) K70 was a critical determinant of mitochondrial permeability transition pore (mPTP) sensitivity.
A, Docking of C-V adenosine triphosphate (ATP) synthase (PDB: 2WSS) and cyclophilin D (CypD; yellow, PDB: 2BIU) with Patch-Dock and predefined constraint (see Methods). Left: overall view of OSCP and CypD interface with acetylated lysine residues highlighted as magenta spheres. Two lysines are located at the predicted interaction interface (black box). Right: magnified image of the putative interaction interface depicting the proposed regulation of interaction by acetylation on K70 of OSCP and K66 of CypD (magenta sticks). The distance between the 2 ε-nitrogen atoms of K70 of OSCP and K66 of CypD is measured by PyMOL (dotted line). **B,** Expression vectors indicated were transfected into HEK293 cells. Cell lysates were immunoprecipitated by ATP synthase antibodies and the presence of OSCP, HA-tagged OSCP and CypD was assessed by Western blot. Em indicates empty pcDNA3.1 vector transfected; K, wild-type HA-tagged OSCP; Q, K70Q mutant of OSCP; R, K70R of OSCP; and U: untransfected. Representative blots from at least 3 independent experiments were shown in **B**. **C,** Representative calcium-stimulated mPTP opening of permeabilized HEK293 cells after transfections were shown. CsA (1 uM) was added after permeabilization of untransfected HEK293 cells. Arrows represent each 5 nmol calcium pulse.

determine the significance of OSCP-K70Ac, wild-type (K), K70Q (Q), and K70R (R) mutants of OSCP-K70 were expressed in HEK293 cells (Figure VIIE in the online-only Data Supplement). Expression of acetylation-mimetic K70Q mutant showed increased interaction with CypD and sensitized mPTP opening (lowered calcium retention capacity), while expression of acetylation-insensitive K70R showed the opposite effects (Figure 7B-C, Figure VIIF-G in the online-only Data Supplement). The data collectively indicate a critical role of OSCP-K70Ac in determining mPTP sensitivity via its interaction with CypD.

DISCUSSION

In this study we demonstrated that protein hyperacetylation induced by mitochondrial dysfunction is a positive regulator of pathologic remodeling in mouse hearts with primary or acquired mitochondrial dysfunction as well as in human failing hearts. Our study identified 2 distinct mechanisms that hyper-

acetylated protein targets, ie, the MAS and the regulators of mPTP, mediate increased propensity to heart failure. Importantly, we demonstrated that normalization of NADH/NAD+ ratio in the heart by genetic or pharmacologic approaches alleviated hyperacetylation, abrogated the 2 pathogenic mechanisms, and blunted the course of heart failure in mouse models, thus suggesting a novel therapy for heart failure.

Mitochondrial dysfunction has been recognized as a maladaptive mechanism during the development of heart failure.[3,4] However, there has been no effective therapy in the clinic.[5] Based on findings obtained from a genetic model of defective mitochondrial function, the present study identified and targeted pathogenic mechanisms caused by the imbalance of NADH production and oxidation in the mitochondria of hypertrophied and failing heart. We found that expanding the NAD+ pool could normalize NADH/NAD+ ratio, restore protein acetylation, and mitigate the development of heart failure in multiple mouse models of pathologic hypertrophy and

failure. The strategy represents a novel therapeutic approach that targets the modification of protein functions consequent of mitochondrial dysfunction. Indeed, the NAD+ precursors such as NMN or nicotinamide riboside have yielded beneficial outcomes in animal models of diabetes mellitus,[38] obesity,[39] and aging.[40] By comparing mouse models and human failing hearts in this study, we provide strong evidence that a similar mechanism applies to human heart failure, and indicate a highly translatable therapeutic strategy. Although NMN has poor oral bioavailability, oral administration of nicotinamide riboside, a recently approved nutritional supplement, is effective in rising blood NAD+ levels in healthy volunteers (Airhart et al, unpublished). Additional study of the safety and tolerability of expanding NAD+ pool in patient population is thus highly warranted.

Previous studies have shown that the level of protein acetylation is related closely to the metabolic state of the cell, and it fluctuates with nutritional status.[41] Persistent hyperacetylation in the heart, such as in mice with deletion of Sirt3 or Ndusf4, resulted in increased sensitivity to stress while the unstressed heart is normal.[10,36] We previously observed that increased NADH/NAD+ ratio in the Ndusf4 deficient heart inhibited Sirt3 resulting in protein hyperacetylation.[10] Restoring Sirt3 activity through normalization of NADH/NAD+ ratio in this study reverses mitochondrial protein hyperacetylation in cKO hearts as well as in hearts with pathologic hypertrophy by pressure overload or isoproterenol stimulation. Acetylome analyses from studies of Sirt3-null mice[42–44] and failing hearts[45] have identified thousands of mitochondrial acetylation sites, but only a handful of their functions have been biochemically characterized. The specific mechanisms connecting protein acetylation and increased sensitivity to stress remain to be poorly understood. Here we identified a subgroup of mitochondrial proteins that are highly sensitive to NADH/NAD+ ratio, among which hyperacetylation of malate aspartate shuttle and regulators of mPTP were shown to be linked causally to the development of heart failure. Furthermore, by expanding the NAD+ pool we were able to normalize but not overcorrect the NADH/NAD+ ratio, suggesting that such an approach is desirable from bioenergetics point of view.

It is conceivable that the disease mechanisms mediated by protein hyperacetylation involve other protein targets beyond the 2 groups reported here. Previous studies have identified other molecular targets of acetylation which are sensitive to NAD+ precursor supplementation in diabetes and mitochondrial diseases.[38–40] Furthermore, we found that downregulation of malate aspartate shuttle (MAS) activity resulted in significant changes of cytosolic redox state. The MAS transfers the electron from NADH generated by glycolysis into mitochondria. Inhibition of MAS by acetylation serves as a feedback mechanism to protect mitochondrial compartment from further increases in NADH/NAD+ ratio but at the cost of altering cytosolic redox environment and sirtuin activities in the nonmitochondrial compartment. In addition, multiple redox dependent regulatory mechanisms, such as cysteine oxidation, glutathionylation, redox-mediated phosphorylation, have been shown to play important roles in the development of cardiac dysfunction.[46,47] Of note, ATP citrate lyase, an enzyme that catalyzes the cytoplasmic conversion of mitochondrial citrate into the acetyl-coa in the cytosol, is activated at reduced state,[48] thus increasing substrate supply for protein acetylation. Consistently, a significant number of hyperacetylated proteins are found in the nonmitochondrial compartments of the complex-I deficient hearts, suggesting that mitochondrial dysfunction ultimately could affect whole cell acetylation. Although the scope of this study did not allow us to determine the specific contribution by each of these mechanisms in the progression of heart failure, it provides compelling evidence for targeting NADH/NAD+ ratio for therapy. Moreover, observations made here open a new avenue for investigating mitochondrial-cytosolic redox communications in chronic diseases involving mitochondrial dysfunction.

Cell death caused by the opening of mitochondrial permeability transition pore (mPTP) is an important mechanism in the development of heart failure. We and others have shown previously that increased mitochondrial protein acetylation sensitizes the mPTP,[10,36] but the specific molecular targets are unknown due to the lack of physical identity of the mPTP. By combining the computational and mutagenesis approaches, we identified the acetylation of K70 on OSCP as a key determinant of mPTP sensitivity via its interaction of CypD. This finding also reconciles with prior reports suggesting that acetylation of CypD at K166 could increase the sensitivity of mPTP.[36] Our computation models propose that acetylation of several lysine residues on CypD, including K66 that is at the closest proximity and K166 that is present at the putative interface of one top scoring model, could further reduce the repulsion between the 2 proteins. OSCP is located at the matrix side of the F_1 subcomplex of the ATP synthase, making stable interaction with proteins of both F1 and the peripheral stalk (Figure VIB-C in the online-only Data Supplement). Recent studies suggest that either the dimer of F_1F_0-ATP synthase[31] or F_0 sub-complex[49,50] forms the mPTP under specific conditions. Our results, although in line with this model, do not confirm the specific identity of the physical pore. They, nevertheless, provide a novel target to manipulate the mPTP sensitivity for therapy.

In summary, using a mouse model of mitochondrial complex-I deficiency as the discovery tool we have unveiled novel mechanisms by which mitochondrial dysfunction modulates cellular stress response through NADH/NAD+-sensitive protein acetylation. The findings were validated in multiple mouse models of pathological hypertrophy, as well as in human failing hearts. Our pre-

clinical data not only demonstrate a clear benefit of expanding NAD+ pool in heart failure therapy, the currently available NAD+ precursor compounds, but also make our findings immediately translatable.

ACKNOWLEDGMENTS

SOURCES OF FUNDING

DISCLOSURES

None.

AFFILIATIONS

From Mitochondria and Metabolism Center (C.F.L., L.G.-M., Y.C., N.D.R., R.T.), Department of Anesthesiology and Pain Medicine (C.F.L., L.G.-M, Y.C., N.D.R., R.T.), Department of Genome Sciences (J.D.C., J.E.B.), Department of Pathology (Y.A.C.), and Department of Medicinal Chemistry (J.S.E., Y.A.G., D.R.G.), University of Washington, Seattle, WA.

FOOTNOTES

REFERENCES

1. Roth GA, Forouzanfar MH, Moran AE, Barber R, Nguyen G, Feigin VL, Naghavi M, Mensah GA, Murray CJ. Demographic and epidemiologic drivers of global cardiovascular mortality. N Engl J Med. 2015;372:1333–1341. doi: 10.1056/NEJMoa1406656.

2. Mozaffarian D, Benjamin EJ, Go AS, Arnett DK, Blaha MJ, Cushman M, Das SR, de Ferranti S, Despres JP, Fullerton HJ, Howard VJ, Huffman MD, Isasi CR, Jimenez MC, Judd SE, Kissela BM, Lichtman JH, Lisabeth LD, Liu S, Mackey RH, Magid DJ, McGuire DK, Mohler ER, 3rd, Moy CS, Muntner P, Mussolino ME, Nasir K, Neumar RW, Nichol G, Palaniappan L, Pandey DK, Reeves MJ, Rodriguez CJ, Rosamond W, Sorlie PD, Stein J, Towfighi A, Turan TN, Virani SS, Woo D, Yeh RW, Turner MB, American Heart Association statistics C and stroke statistics S. Heart disease and stroke statistics 2016 update: a report from the American Heart Association. Circulation. 2016;133:e38–e360.

3. Bayeva M, Gheorghiade M, Ardehali H. Mitochondria as a therapeutic target in heart failure. J Am Coll Cardiol. 2013;61:599–610. doi: 10.1016/j.jacc.2012.08.1021.

4. Rosca MG, Tandler B, Hoppel CL. Mitochondria in cardiac hypertrophy and heart failure. J Mol Cell Cardiol. 2013;55:31–41. doi: 10.1016/j.yjmcc.2012.09.002.

5. Wang W, Karamanlidis G, Tian R. Novel targets for mitochondrial medicine. Sci Transl Med. 2016;8:326rv3. doi: 10.1126/scitranslmed.aac7410.

6. Choudhary C, Weinert BT, Nishida Y, Verdin E, Mann M. The growing landscape of lysine acetylation links metabolism and cell signalling. Nat Rev Mol Cell Biol. 2014;15:536–550. doi: 10.1038/nrm3841.

7. Cantó C, Menzies KJ, Auwerx J. NAD(+) metabolism and the control of energy homeostasis: a balancing act between Mitochondria and the nucleus. Cell Metab. 2015;22:31–53. doi: 10.1016/j.cmet.2015.05.023.

8. Lee CF, Tian R. Mitochondrion as a target for heart failure therapy—role of protein lysine acetylation. Circ J. 2015;79:1863–1870. doi: 10.1253/circj.CJ-15-0742.

9. Sauve AA, Wolberger C, Schramm VL, Boeke JD. The biochemistry of sirtuins. Annu Rev Biochem. 2006;75:435–465. doi: 10.1146/annurev.biochem.74.082803.133500.

10. Karamanlidis G, Lee CF, Garcia-Menendez L, Kolwicz SC Jr, Suthammarak W, Gong G, Sedensky MM, Morgan PG, Wang W, Tian R. Mitochondrial complex I deficiency increases protein acetylation and accelerates heart failure. Cell Metab. 2013;18:239–250. doi: 10.1016/j.cmet.2013.07.002.

11. Kolwicz SC Jr, Olson DP, Marney LC, Garcia-Menendez L, Synovec RE, Tian R. Cardiac-specific deletion of acetyl CoA carboxylase 2 prevents metabolic remodeling during pressure-overload hypertrophy. Circ Res. 2012;111:728–738. doi: 10.1161/CIRCRESAHA.112.268128.

12. Boehm EA, Jones BE, Radda GK, Veech RL, Clarke K. Increased uncoupling proteins and decreased efficiency in palmitate-perfused hyperthyroid rat heart. Am J Physiol Heart Circ Physiol. 2001;280:H977–H983.

13. Keller A, Nesvizhskii AI, Kolker E, Aebersold R. Empirical statistical model to estimate the accuracy of peptide identifications made by MS/MS and database search. Anal Chem. 2002;74:5383–5392.

14. Nesvizhskii AI, Keller A, Kolker E, Aebersold R. A statistical model for identifying proteins by tandem mass spectrometry. Anal Chem. 2003;75:4646–4658.

15. Elias JE, Gygi SP. Target-decoy search strategy for increased confidence in large-scale protein identifications by mass spectrometry. Nat Methods. 2007;4:207–214. doi: 10.1038/nmeth1019.

16. Ma K, Vitek O, Nesvizhskii AI. A statistical model-building perspective to identification of MS/MS spectra with PeptideProphet. BMC Bioinformatics. 2012;13 Suppl 16:S1. doi: 10.1186/1471-2105-13-S16-S1.

17. Liu H, Sadygov RG, Yates JR 3rd. A model for random sampling and estimation of relative protein abundance in shotgun proteomics. Anal Chem. 2004;76:4193–4201. doi: 10.1021/ac0498563.

18. Eng JK, Jahan TA, Hoopmann MR. Comet: an open-source MS/MS sequence database search tool. Proteomics. 2013;13:22–24. doi: 10.1002/pmic.201200439.

19. Siegel S and Castellan Jr. NJ. Nonparametric Statistics for the Behavioral Sciences. Second Edition ed: McGraw Hill; 2000.

20. Hsu CP, Oka S, Shao D, Hariharan N, Sadoshima J. Nicotinamide phosphoribosyltransferase regulates cell survival through NAD+ synthesis in cardiac myocytes. Circ Res. 2009;105:481–491. doi: 10.1161/CIRCRESAHA.109.203703.

21. Errami M, Galindo CL, Tassa AT, Dimaio JM, Hill JA, Garner HR. Doxycycline attenuates isoproterenol- and transverse aortic band-

ing-induced cardiac hypertrophy in mice. *J Pharmacol Exp Ther.* 2008;324:1196–1203. doi: 10.1124/jpet.107.133975.

22. Houtkooper RH, Cantó C, Wanders RJ, Auwerx J. The secret life of NAD+: an old metabolite controlling new metabolic signaling pathways. *Endocr Rev.* 2010;31:194–223. doi: 10.1210/er.2009-0026.

23. LaNoue KF, Williamson JR. Interrelationships between malate-aspartate shuttle and citric acid cycle in rat heart mitochondria. *Metabolism.* 1971;20:119–140.

24. Allard MF, Schönekess BO, Henning SL, English DR, Lopaschuk GD. Contribution of oxidative metabolism and glycolysis to ATP production in hypertrophied hearts. *Am J Physiol.* 1994;267(2 Pt 2):H742–H750.

25. Nascimben L, Ingwall JS, Lorell BH, Pinz I, Schultz V, Tornheim K, Tian R. Mechanisms for increased glycolysis in the hypertrophied rat heart. *Hypertension.* 2004;44:662–667. doi: 10.1161/01.HYP.0000144292.69599.0c.

26. Wambolt RB, Lopaschuk GD, Brownsey RW, Allard MF. Dichloroacetate improves postischemic function of hypertrophied rat hearts. *J Am Coll Cardiol.* 2000;36:1378–1385.

27. Rupert BE, Segar JL, Schutte BC, Scholz TD. Metabolic adaptation of the hypertrophied heart: role of the malate/aspartate and alpha-glycerophosphate shuttles. *J Mol Cell Cardiol.* 2000;32:2287–2297. doi: 10.1006/jmcc.2000.1257.

28. Lewandowski ED, O'donnell JM, Scholz TD, Sorokina N, Buttrick PM. Recruitment of NADH shuttling in pressure-overloaded and hypertrophic rat hearts. *Am J Physiol Cell Physiol.* 2007;292:C1880–C1886. doi: 10.1152/ajpcell.00576.2006.

29. Baines CP, Kaiser RA, Purcell NH, Blair NS, Osinska H, Hambleton MA, Brunskill EW, Sayen MR, Gottlieb RA, Dorn GW, Robbins J, Molkentin JD. Loss of cyclophilin D reveals a critical role for mitochondrial permeability transition in cell death. *Nature.* 2005;434:658–662. doi: 10.1038/nature03434.

30. Nakagawa T, Shimizu S, Watanabe T, Yamaguchi O, Otsu K, Yamagata H, Inohara H, Kubo T, Tsujimoto Y. Cyclophilin D-dependent mitochondrial permeability transition regulates some necrotic but not apoptotic cell death. *Nature.* 2005;434:652–658. doi: 10.1038/nature03317.

31. Giorgio V, von Stockum S, Antoniel M, Fabbro A, Fogolari F, Forte M, Glick GD, Petronilli V, Zoratti M, Szabó I, Lippe G, Bernardi P. Dimers of mitochondrial ATP synthase form the permeability transition pore. *Proc Natl Acad Sci U S A.* 2013;110:5887–5892. doi: 10.1073/pnas.1217823110.

32. Chinopoulos C, Adam-Vizi V. Modulation of the mitochondrial permeability transition by cyclophilin D: moving closer to F(0)-F(1) ATP synthase? *Mitochondrion.* 2012;12:41–45. doi: 10.1016/j.mito.2011.04.007.

33. Schlatter D, Thoma R, Küng E, Stihle M, Müller F, Borroni E, Cesura A, Hennig M. Crystal engineering yields crystals of cyclophilin D diffracting to 1.7 A resolution. *Acta Crystallogr D Biol Crystallogr.* 2005;61(Pt 5):513–519. doi: 10.1107/S0907444905003070.

34. Rees DM, Leslie AG, Walker JE. The structure of the membrane extrinsic region of bovine ATP synthase. *Proc Natl Acad Sci U S A.* 2009;106:21597–21601. doi: 10.1073/pnas.0910365106.

35. Schneidman-Duhovny D, Inbar Y, Nussinov R, Wolfson HJ. PatchDock and SymmDock: servers for rigid and symmetric docking. *Nucleic Acids Res.* 2005;33(Web Server issue):W363–W367. doi: 10.1093/nar/gki481.

36. Hafner AV, Dai J, Gomes AP, Xiao CY, Palmeira CM, Rosenzweig A, Sinclair DA. Regulation of the mPTP by SIRT3-mediated deacetylation of CypD at lysine 166 suppresses age-related cardiac hypertrophy. *Aging (Albany NY).* 2010;2:914–923. doi: 10.18632/aging.100252.

37. Bochaton T, Crola-Da-Silva C, Pillot B, Villedieu C, Ferreras L, Alam MR, Thibault H, Strina M, Gharib A, Ovize M, Baetz D. Inhibition of myocardial reperfusion injury by ischemic postconditioning requires sirtuin 3-mediated deacetylation of cyclophilin D. *J Mol Cell Cardiol.* 2015;84:61–69. doi: 10.1016/j.yjmcc.2015.03.017.

38. Yoshino J, Mills KF, Yoon MJ, Imai S. Nicotinamide mononucleotide, a key NAD(+) intermediate, treats the pathophysiology of diet- and age-induced diabetes in mice. *Cell Metab.* 2011;14:528–536. doi: 10.1016/j.cmet.2011.08.014.

39. Cantó C, Houtkooper RH, Pirinen E, Youn DY, Oosterveer MH, Cen Y, Fernandez-Marcos PJ, Yamamoto H, Andreux PA, Cettour-Rose P, Gademann K, Rinsch C, Schoonjans K, Sauve AA, Auwerx J. The NAD(+) precursor nicotinamide riboside enhances oxidative metabolism and protects against high-fat diet-induced obesity. *Cell Metab.* 2012;15:838–847. doi: 10.1016/j.cmet.2012.04.022.

40. Gomes AP, Price NL, Ling AJ, Moslehi JJ, Montgomery MK, Rajman L, White JP, Teodoro JS, Wrann CD, Hubbard BP, Mercken EM, Palmeira CM, de Cabo R, Rolo AP, Turner N, Bell EL, Sinclair DA. Declining NAD(+) induces a pseudohypoxic state disrupting nuclear-mitochondrial communication during aging. *Cell.* 2013;155:1624–1638. doi: 10.1016/j.cell.2013.11.037.

41. Yang L, Vaitheesvaran B, Hartil K, Robinson AJ, Hoopmann MR, Eng JK, Kurland IJ, Bruce JE. The fasted/fed mouse metabolic acetylome: N6-acetylation differences suggest acetylation coordinates organ-specific fuel switching. *J Proteome Res.* 2011;10:4134–4149. doi: 10.1021/pr200313x.

42. Hirschey MD, Shimazu T, Goetzman E, Jing E, Schwer B, Lombard DB, Grueter CA, Harris C, Biddinger S, Ilkayeva OR, Stevens RD, Li Y, Saha AK, Ruderman NB, Bain JR, Newgard CB, Farese RV Jr, Alt FW, Kahn CR, Verdin E. SIRT3 regulates mitochondrial fatty-acid oxidation by reversible enzyme deacetylation. *Nature.* 2010;464:121–125. doi: 10.1038/nature08778.

43. Qiu X, Brown K, Hirschey MD, Verdin E, Chen D. Calorie restriction reduces oxidative stress by SIRT3-mediated SOD2 activation. *Cell Metab.* 2010;12:662–667. doi: 10.1016/j.cmet.2010.11.015.

44. Shimazu T, Hirschey MD, Hua L, Dittenhafer-Reed KE, Schwer B, Lombard DB, Li Y, Bunkenborg J, Alt FW, Denu JM, Jacobson MP, Verdin E. SIRT3 deacetylates mitochondrial 3-hydroxy-3-methylglutaryl CoA synthase 2 and regulates ketone body production. *Cell Metab.* 2010;12:654–661. doi: 10.1016/j.cmet.2010.11.003.

45. Horton JL, Martin OJ, Lai L, Riley NM, Richards AL, Vega RB, Leone TC, Pagliarini DJ, Muoio DM, Bedi KC, Jr., Margulies KB, Coon JJ and Kelly DP. Mitochondrial protein hyperacetylation in the failing heart. *JCI Insight.* 2016;2:e84897.

46. Chung HS, Wang SB, Venkatraman V, Murray CI, Van Eyk JE. Cysteine oxidative posttranslational modifications: emerging regulation in the cardiovascular system. *Circ Res.* 2013;112:382–392. doi: 10.1161/CIRCRESAHA.112.268680.

47. Murphy E, Kohr M, Menazza S, Nguyen T, Evangelista A, Sun J, Steenbergen C. Signaling by S-nitrosylation in the heart. *J Mol Cell Cardiol.* 2014;73:18–25. doi: 10.1016/j.yjmcc.2014.01.003.

48. Wells TN, Saxty BA. Redox control of catalysis in ATP-citrate lysate from rat liver. *Eur J Biochem.* 1992;204:249–255.

49. Alavian KN, Beutner G, Lazrove E, Sacchetti S, Park HA, Licznerski P, Li H, Nabili P, Hockensmith K, Graham M, Porter GA Jr, Jonas EA. An uncoupling channel within the c-subunit ring of the F1FO ATP synthase is the mitochondrial permeability transition pore. *Proc Natl Acad Sci U S A.* 2014;111:10580–10585. doi: 10.1073/pnas.1401591111.

50. Bonora M, Bononi A, De Marchi E, Giorgi C, Lebiedzinska M, Marchi S, Patergnani S, Rimessi A, Suski JM, Wojtala A, Wieckowski MR, Kroemer G, Galluzzi L, Pinton P. Role of the c subunit of the FO ATP synthase in mitochondrial permeability transition. *Cell Cycle.* 2013;12:674–683. doi: 10.4161/cc.23599.

Circulation

Normalization of NAD$^+$ Redox Balance as a Therapy for Heart Failure

Chi Fung Lee, Juan D. Chavez, Lorena Garcia-Menendez, Yongseon Choi, Nathan D. Roe, Ying Ann Chiao, John S. Edgar, Young Ah Goo, David R. Goodlett, James E. Bruce and Rong Tian

The online version of this article, along with updated information and services, is located on the World Wide Web at:
http://circ.ahajournals.org/content/134/12/883

Data Supplement (unedited) at:
http://circ.ahajournals.org/content/suppl/2016/08/03/CIRCULATIONAHA.116.022495.DC1.html

Supplementary material

Supplemental figure and figure legends

Figure S1, related to Fig 1
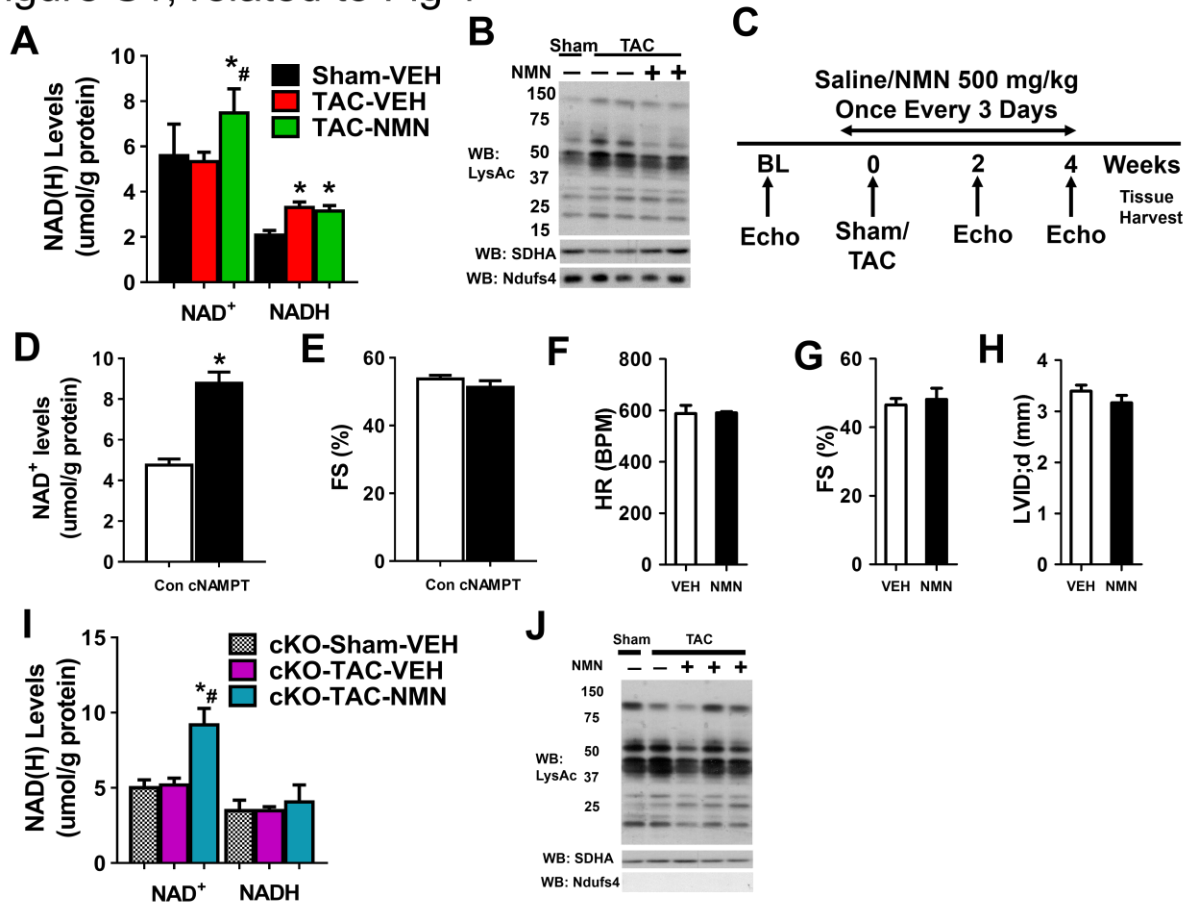
Figure S1. **Effects of elevation of cardiac NAD⁺ levels by NMN administration on acetylation and cardiac function. (A)** NAD(H) levels from mitochondria of control mice after sham or TAC surgeries with and without NMN treatment were measured. *: P<0.05 compared to Sham-VEH. #: P<0.05 compared to TAC-VEH. **(B)** Representative Western Blotting of acetylation of mitochondria isolated as indicated. **(C)** Experimental plan for sham/TAC surgeries, treatments, and echocardiography (echo). **(D)** NAD⁺ levels and **(E)** fractional shortening (FS) of control and cNAMPT hearts were measured. N=3. *: P<0.05 compared to Control. **(F)** Heart rate (HR), **(G)** FS, **(H)** left ventricle

internal dimension at diastole (LVID;d) of vehicle (VEH, saline) or NMN (500 mg/kg) treated cKO mice were measured. N=3. NAD(H) levels of cKO hearts after sham or TAC surgeries and NMN treatment were measured. **(I)** NAD(H) levels of cKO hearts after sham or TAC surgeries and NMN treatment were measured. **(J)** Representative Western Blots measuring acetylation, SDHA and Ndufs4 levels of mitochondria isolated as indicated. N=3-4. *: $P<0.05$ compared to corresponding Sham; #: $P<0.05$ compared to corresponding TAC. Data are expressed as means ±SEM.

Figure S2 related to Fig 2
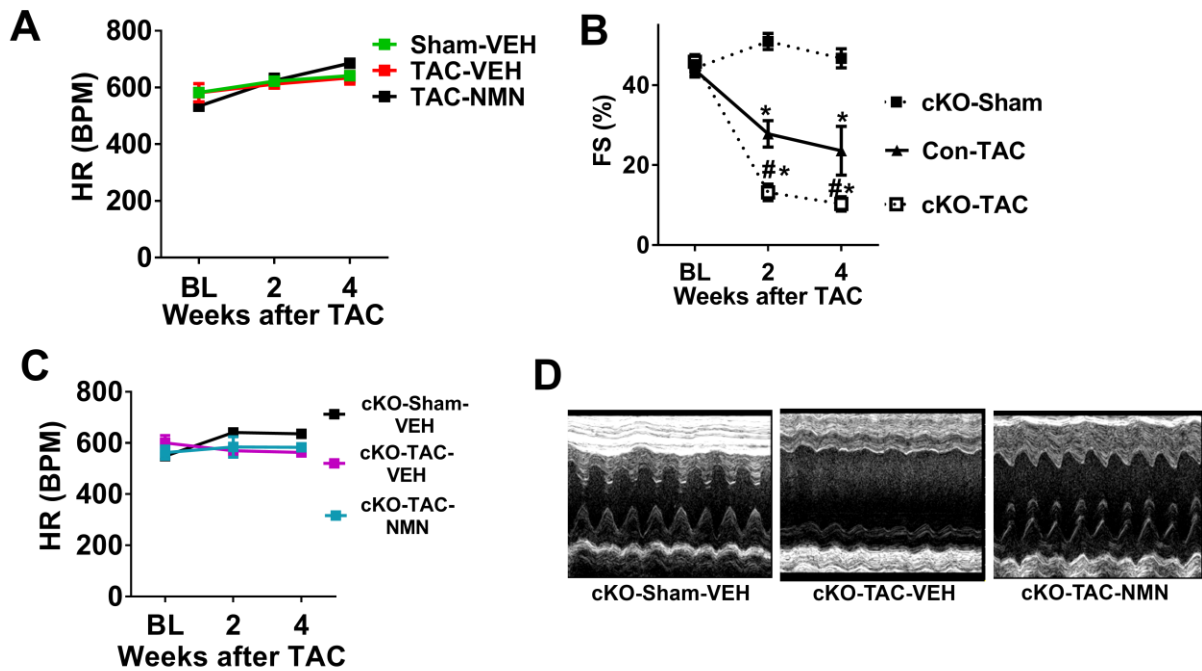
Figure S2. **Effects of NMN treatment on cardiac function after TAC. (A)** Heart rate (HR) of control mice after sham or TAC surgeries with and without NMN treatment were recorded. N=4-8. **(B)** FS of control and cKO mice after Sham/TAC surgeries at baseline (BL), 2 and 4 weeks after TAC. N=5-8. *: P<0.05 compared to cKO-Sham; #: P<0.05 compared to Con-TAC. **(C)** HR of cKO mice treated as indicated were assessed. N=5-6. **(D)** Representative M-mode images from mice indicated. Data are expressed as means ±SEM.

Figure S3, related to Fig 3
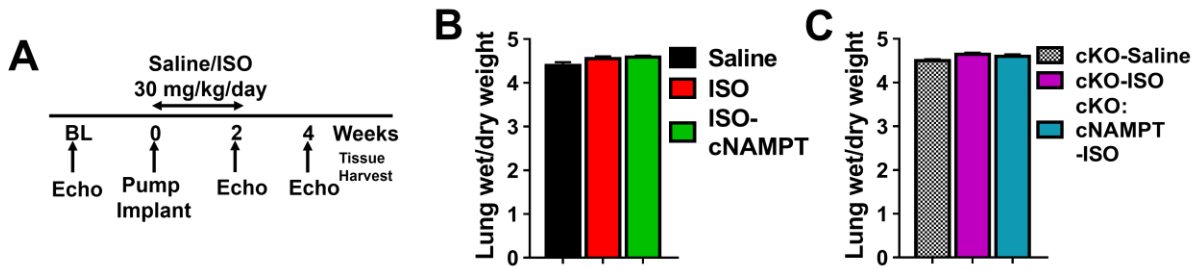
Figure S3. **Effect of cNAMPT expression on lung edema of mice after isoproterenol stimulation. (A)** Experimental plan for saline/ISO treatment and echocardiography (echo). **(B-C)** The ratio of wet/dry lung weight of indicated mice were measured. N=5-9. Data are expressed as means ±SEM.

Figure S4, related to Fig. 4
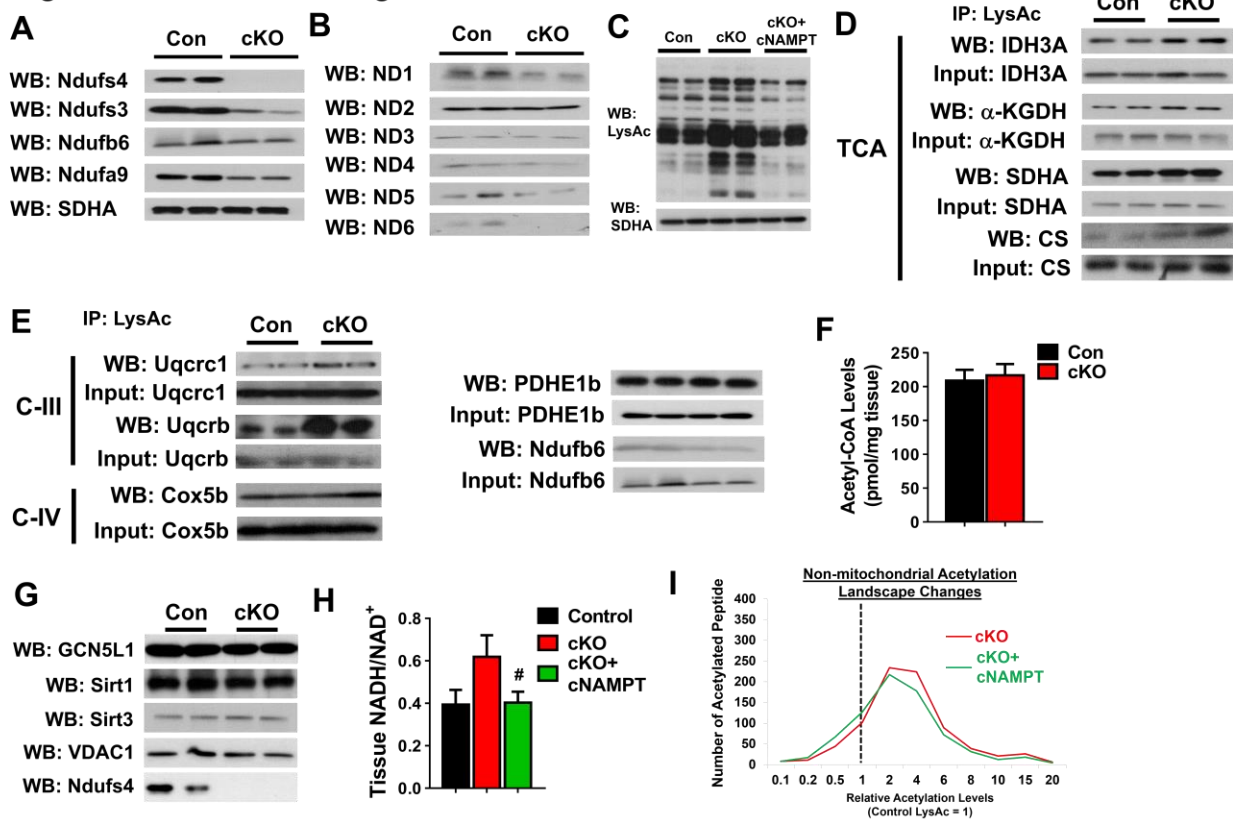
Figure S4. **Complex I proteins, acetylation of mitochondrial proteins, acetyl-coA, Sirtuins and GCN5L1 levels in cKO and effects of cNAMPT on acetylation landscape.** Representative Western blots of C-I proteins contributed from **(A)** nuclear and **(B)** mitochondrial genomes from control and cKO mitochondrial lysates. N=4. **(C)** Representative Western blot for ac levels of indicated hearts. Acetylation levels of **(D)** TCA, **(E)** ETC proteins, PDHE1b and Ndufs6 were assessed by immunoprecipitation/Western blot (IP-WB) analysis. N=4. **(F)** Acetyl-coA levels of cardiac tissues as indicated were measured. N=4. **(G)** Protein levels of mitochondrial acetyltransferase GCN5L1, and deacetylases Sirt1/3, in control or cKO mitochondria were measured. VDAC and Ndufs4 as controls. **(H)** Tissue NADH/NAD$^+$ ratio of indicated hearts were measured and **(I)** Non-mitochondrial acetylation landscape

changes of cKO and cKO+cNAMPT hearts were compared. N=4. #: P<0.05 compared to cKO. Data are expressed as means ±SEM.

Figure S5, related to Fig. 5
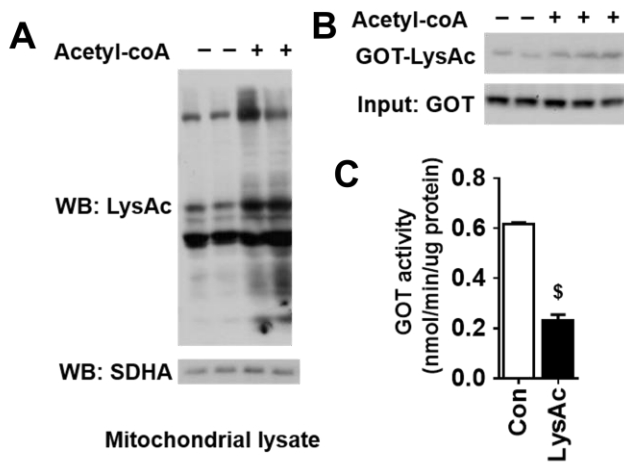
Figure S5. In vitro acetylation of mitochondrial proteins by acetyl-coA. (A)

Mitochondrial lysates were incubated with or without acetyl-coA (1.5 mM) for six hours

and acetylation levels were probed with anti-acetyl-lysine antibody. **(B)** The acetyl-coA-

treated mitochondrial lysates were immunoprecipitated with anti-acetyl-lysine antibody

coupled agarose and probed for the presence of GOT2 protein. **(C)** The GOT activities

of the non-acetylated and acetylated lysates were measured.

Figure S6, related to Fig. 6
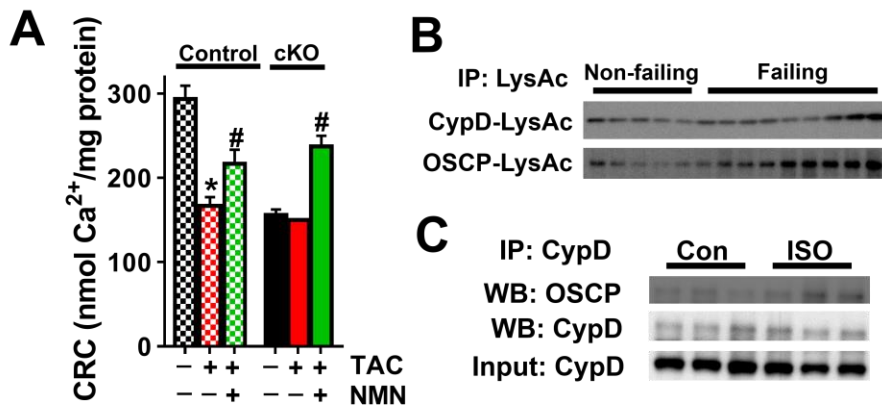
Figure S6. **Sensitivity of mPTP linked to OSCP and CypD acetylation. (A)** Calcium

retention capacity (CRC) of isolated mitochondria as indicated was quantified. N=3-4. *:

$P<0.05$ compared to corresponding Sham; #: $P<0.05$ compared to corresponding TAC-

VEH. **(B)** Acetylation of CypD and OSCP in normal and failing human hearts were

determined by IP-WB. **(C)** Interaction of CypD and OSCP in hypertrophic hearts

induced by ISO was determined by IP-WB. Data are expressed as means ±SEM.

Figure S7, related to Fig. 7
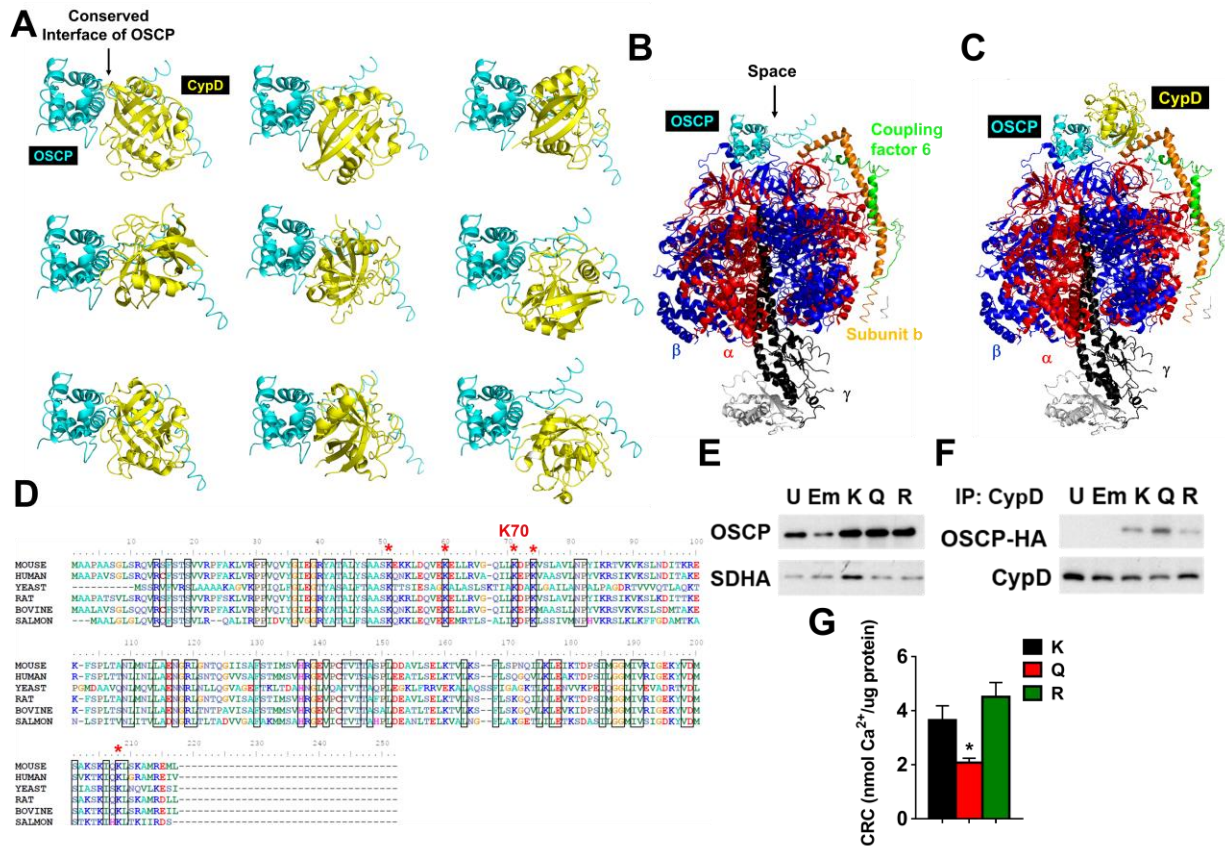
Figure S7. **Structure-function relationship of OSCP-K70Ac with mPTP sensitivity.**

(A) Nine highest scored docking solutions between OSCP (chain S only of 2WSS) and CypD (2BIU). OSCP protein orientations were similar in these solutions and in OSCP of panel B-C. **(B)** Picture depicting F_1F_0-ATP synthase complex (PDB: from 2WSS). A space is present allowing binding of CypD to the conserved interface of OSCP identified in (A). Alpha subunit: red. Beta subunit: blue. Gamma subunit: black. Coupling factor 6: green. Subunit b: orange. OSCP: cyan. **(C)** Picture showing one of the docking solutions of CypD with F_1F_0-ATP synthase complex. **(D)** Sequence alignment of OSCP proteins from mouse, human, yeast, rat, bovine and salmon shows OSCP-K70 is highly conserved among species (red asterisks) while other lysines may not. **(E)** Expression

levels and **(F)** interaction of OSCP-CypD of wild-type (K), K70Q (Q), and K70R (R) of

OSCP variants in HEK293 cells were determined by Western blot. U: untransfected

HEK293 cells. Em: empty pcDNA3.1 vector transfected cells. **(G)** CRC of permeabilized

HEK293 cells treated as indicated were quantified. N=4-5. *: $P<0.05$ corresponding to K.

Data are expressed as means ±SEM.

Supplementary table legends

Supplementary Table 1: clinical data of the human subjects. ICM: ischemic cardiomyopathy. DCM: dilated cardiomyopathy. BMI: body mass index. EF: ejection fraction.

Supplementary Table 2: list of C-I proteins showed significant changes in levels from mitochondrial proteome analysis (cKO/Con > 2 or < 0.5; P<0.01, n=4).

Supplementary Table 3: list of cardiac mitochondrial proteins identified and spectral count values.

Supplementary Table 4: acetylated lysine sites of malate aspartate shuttle (MAS) proteins. K[170.11] depicts acetylation site. N/A: no peptide identified in Control but in cKO. N/D: not determined.

Supplementary Table 5: acetylated lysine sites of proteins linked to mPTP. K[170.11] depicts acetylation site. N/A: no peptide identified in Control but in cKO. N/D: not determined.

Supplementary methods

Animal care, surgical procedures and echocardiography

All procedures involving animal use were performed with the approval of IACUC of the University of Washington. Cardiac specific Ndufs4-KO mice (cKO) were generated as described [1]. Mice over-expressing NAMPT under the control of a-MHC promoter (cNAMPT) [2] were crossed with cKO to generate the desired genotypes as used in the experiments. Male mice (3-4 months old) underwent transverse aortic constriction (TAC) or sham surgery. Mice were anesthetized with sodium pentobarbital (75 mg/kg). Aorta

was exposed via a left thoracotomy and a constriction was made using a 7-0 ligature around the vessel and tied against a 27-gauge blunt needle. Sham surgeries were performed as above without performing the constriction of the aorta. NMN were delivered intraperitoneally to mice at 500 mg/kg once every three days 5-day before surgeries and 4-week after surgeries. Saline were delivered as control treatment. Echocardiography of hearts was performed at indicated time after surgery using the VEVO 770 system with a 707B scan head to lightly-anesthetized mice. Measurements were made when heart rate was within 500-600 bpm. Cardiac function and geometry measurements were measured in parasternal long axis B- and M-mode images and calculated by average of at least three cardiac cycles and carried out in a blind fashion. For experiments that mice were stressed by isoproterenol (30 mg/kg/day), isoproterenol was delivered by osmotic minipump (Alzet) for 2 weeks. Cardiac echocardiography was measured at baseline, 2-week and 4-week after implantation. Minipumps carrying saline were used as control. Hearts were harvested for mitochondrial isolated and subsequent biochemical assays.

Ex vivo measurements of cardiac function and energetics

Langendorff perfused mouse hearts were isolated as previously described [3, 4] and maintained at a constant perfusion pressure of 80 mmHg at 37°C. Hearts were perfused with a buffer containing in mM; EDTA 0.5, KCl 5.3, $MgSO_4$ 1.2, NaCl 118, $NaHCO_3$ 25, $CaCl_2$ 2, mixed fatty acids 0.4 (bound to 1.2% albumin), Glucose 5.5, Lactate 1.2, and Insulin 50 mU/L. After an equilibration period of 30 minutes, hearts were switched to a buffer containing 4mM $CaCl_2$ to increase cardiac workload for 30 minutes. Left

ventricular function was monitored by a powerlab (AD Instruments) data acquisition system and high energy phosphate content was evaluated by ^{31}P NMR spectroscopy.

Mitochondrial isolation, proteome, and acetylome analyses

Mitochondria were isolated as described [5]. For mitochondrial proteome analysis by mass spectrometry, 500ug of isolated mitochondria were resuspended in 0.2% SDS in ammonium bicarbonate buffer with protease inhibitor cocktail (Roche) and deacetylase inhibitors (nicotinamide, trichostatin A) and boiled for 5 minutes. The samples were reduced and alkylated with dithiothreitol (DTT) and iodoacetamide (IAA). Samples were diluted to 0.04% SDS and trypsinized with 10 μg of sequencing grade trypsin (Promega) 37 °C overnight. Samples were loaded into MCX column (Waters) and washed by 0.1% and 0.01% trifluoroacetic acid (TFA). Samples were then eluted with 10% NH4OH/90% methanol and dried for MS analysis.

For mass spectrometric analysis of mitochondrial proteome, peptide digestion products were analyzed by electrospray ionization on a linear ion trap Velos mass spectrometer (Thermo Scientific Corp., San Jose, CA). Nanoflow HPLC was performed using a Waters NanoAquity HPLC system (Waters Corporation, Milford, MA). Peptides were trapped on a 100 μm i.d. x 20 mm long precolumn in-house packed with 200 Å (5 μm) Magic C18 particles (C18AQ; Michrom Bioresources Inc., Auburn, CA). Subsequent peptide separation was on an in-house constructed 75 μm i.d. x 180 mm long analytical column pulled using a Sutter Instruments P-2000 CO_2 laser puller (Sutter Instrument Company, Novato, CA) and packed with 100 Å (5 μm) C18AQ particle. For each liquid

chromatography-tandem mass spectrometry (LC-MS/MS) analysis, an estimated amount of 1 µg of peptides (0.1 µg/µL) were loaded on the precolumn at 4 µL/min in water/acetonitrile (95/5) with 0.1% (v/v) formic acid. Peptides were eluted using an acetonitrile gradient flowing at 250 nL/min using mobile phase gradient of 5-35% acetonitrile over 500 min. with a total gradient time of 585 min. Ion source conditions were optimized using the tuning and calibration solution recommended by the instrument provider. Samples were analyzed in duplicates.

Acquired tandem mass spectra were searched for sequence matches against the IPI mouse database using SEQUEST. The following modifications were set as search parameters: peptide mass tolerance at 500 PPM, trypsin digestion cleavage after K or R (except when followed by P), one allowed missed cleavage site, carboxymethylated cysteines (static modification), and oxidized methionines or acetylation on K (variable modification). PeptideProphet [6] and ProteinProphet [7] were used to assign confidence in the identified spectra resulting from the SEQUEST search. It relies on probability models and an Empirical Bayesian approach to model fitting. First a score is produced to reflect the quality of each spectrum. Then a probability-based model is produced for the distribution of correctly and incorrectly identified spectra and fit to the scores of all identified spectra. The confidence in individual spectra are evaluated using the posterior probability. A cutoff is applied on the scores for the set of correctly identified spectra to control the false discovery rate (FDR), defined as the percentage of false positives which pass the cutoff. This method produces a similar estimation of the FDR as the commonly employed target-decoy search strategy [8]. For more details on the statistics

used in the Prophets we refer readers to Ma et al. [9] We used a PeptideProphet probability $\geq$ 0.9 and ProteinProphet probability $\geq$ 0.9 for positive identification at an error rate of less than 1%. Differences in relative expression of proteins were calculated using peptide spectral counting algorithm [10].

For acetylome analysis, whole hearts of different genotypes were lysed with 0.2% SDS buffer with protease inhibitor cocktail (Roche) and deacetylase inhibitors (nicotinamide, trichostatin A). Lysis of heart tissue was aided by repeated freeze-thaw cycles and homogenization. Soluble protein lysates were collected by centrifugation. Protein concentrations of lysates were measured by Lowry assay. 2mg of samples were reduced and alkylated with 5mM DTT and 10mM IAA. The samples were diluted to 0.04% SDS and digested by trypsin. The peptides were cleaned up by MCX cartridge (Waters), eluted with NH_4OH/methanol buffer and dried for IP experiment. Dried samples were re-dissolved in IP buffer (50 mM MOPS pH 7.2, 10 mM $NaPO_4$, 50 mM NaCl). Solubilized peptides were incubated with anti-acetyllysine antibody agarose (Immunechem) for 12 hours at 4 °C with gentle mixing. Agarose was washed with IP buffer and water. Acetylated peptides were eluted by 0.1% TFA in water and dried for MS analysis.

Enriched acetylation peptide samples were analyzed by LC-MS^2 using a Thermo Easy nLC coupled to a Q-Exactive Plus mass spectrometer. Peptide samples were loaded onto a trap column (3 cm x 100 μm i.d.) packed with 5 μm particle size, 200 Å pore size, Magic-C18AQ using a flow rate of 2 μl/min of solvent A (H2O containing 0.1% formic

acid) for a total of 10 min. Peptides were then eluted from the trap column and separated by reversed-phase chromatography over a pulled tip, fused silica analytical column (60 cm 75 μm i.d.) packed with 5 μm particle size, 100 Å pore size, Magic-C18AQ, maintained at 45°C at a flow rate of 300 nL/min using a linear gradient from 90% solvent A/10% solvent B (acetonitrile containing 1% formic acid) to 70% solvent A/30% solvent B over 90 min followed by a 10 min wash with 20% solvent A/80% solvent B. Data dependent analysis (DDA) with the Q-Exactive Plus mass spectrometer consisted of a high resolution (70,000 RP) MS[1] scan followed by MS[2] (17,500) analysis on the 20 most intense precursors. MS[2] settings included an AGC target value of 5×10^4, a normalized collision energy of 25, isolation width of 1.6 *m/z*, activation time of 10 ms, activation Q of 0.25 and a minimum signal threshold of 10,000. Charge state exclusion was singly charged precursor ions, ions with charge state greater than six, and those with an undetermined charge state. Dynamic exclusion was enabled with an exclusion time of 30 s.

Comet (v2013.02 rev1) [11] was used to search the mass spectral data against the UniProt protein database for *Mus musculus* containing forward and reverse sequences (33224 total protein sequences). Comet search parameters included a precursor mass tolerance of 25 ppm, allowing for up to three ^{13}C offset. Trypsin was selected as the digesting enzyme allowing for up to two missed cleavage sites. Variable modifications included oxidation of Met (15.9949 Da) and acetylation on Lys or protein n-termini (42.010565 Da). Static modifications included carbamidomethylation of Cys (57.021464

Da). Fragment ion mass tolerance was set to 0.02 Da. Resulting peptide spectrum matches were filtered to <1% FDR using a forward/reverse sequence strategy.

Label free MS[1] based quantification of peptides was performed using MassChroQ [12]. Retention time alignment between LC-MS data files was performed using the obiwarp method. A 20 ppm tolerance was applied to generate extract ion chromatograms of precursor ions. Peak detection was accomplished using the zivy algorithm with a 30000 detection threshold on the max and a 15000 detection threshold on the min. The cKO/Control ratio of each acetylated peptide was estimated by the average value of four hearts in each animal group. Standard error of the mean was calculated by the error propagation of standard deviation of the peptide in each animal group.

Molecular docking calculation

Crystal structure data from PDB (2BIU and 2WSS, chain S) for CypD and OSCP proteins were subjected to rigid body molecular docking using online platform PATCHDOCK http://bioinfo3d.cs.tau.ac.il/PatchDock/ [13]. The ten highest scoring solutions without applying restriction to calculation were analyzed with the biomolecular visualization tool Pymol to highlight acetylated lysines on the OSCP and CypD complex. The putative interaction interface of OSCP (helix 1 and 5) was consistently observed from the ten solutions and is accessible for CypD binding into the 'space' in the intact F1-ATP synthase structure (Supplementary Fig. 5b,c). Another docking experiment was performed using all chains of 2WSS and 2BIU as input for docking with E36, K37, L40, R41, Q44, K47, L55, K77 on chain S of 2WSS (OSCP) defined as the interaction

interface for CypD from the data of the first round docking. Acetylated lysines identified from proteomics analysis were mapped and specific acetylation of lysines at the interaction interface was determined as in Fig. 4f. Images were generated using Pymol.

Mitochondrial calcium uptake assay and biochemical assays

In mitochondrial calcium uptake assay, 400 mg of mitochondria were incubated in 1-ml cuvette with mitochondrial assay buffer containing 10mM succinate, 120 mM KCl, 10 mM NaCl, 1 mM KH2PO4 and 20 mM HEPES, 1.25 uM Fura FF (Molecular Probes) under constant stirring at 37 °C. 1 mM of CsA was added if indicated. Calcium uptake was initiated with 25 nmol calcium pulse and measured spectroflurometrically. Pulses were added at 2-minute interval until rapid calcium release (mPTP opening) occurred [14]. Calcium retention capacity was calculated as the amount of calcium needed to trigger mPTP opening. For permeabilized HEK293 cells [15], the same setup and buffers were used. HEK293 cells were cultured without serum overnight and cells were lifted and washed with extracellular medium (20 mM HEPES, 120 mM NaCl, 5 mM KCl, 1mM KH_2PO_4, 0.2 mM $MgCl_2$, 0.1 mM EGTA at pH 7.4). Cells were then permeabilized with digitonin (100 ug/ml) in mitochondrial assay buffer. The samples were pulsed with 5 nmol calcium.

$NADH/NAD^+$ levels were measured by assay kit (BioAssay). Malate aspartate shuttle capacities were measured as described [16]. Reaction buffer containing aspartate, ADP, NADH, malate dehydrogenase, glutamic oxaloacetate transaminase was mixed with 10 ug of mitochondria and the change at 340 nm were measured for 4 minutes at 37 °C as baseline oxidation of NADH. Substrate stock containing malate and glutamate were

mixed with mitochondria and reaction buffer and the change at 340 nm were measured as malate/aspartate shuttle-driven oxidation of NADH. Lactate (Trinity Biotech), pyruvate (Abcam), acetyl-coA (Abcam) levels were measured with assay kits. In vitro acetylation of mitochondrial lysate by acetyl-coA was performed in 50 mM HEPES, 150 mM NaCl, pH 8.0 as described before [17]. Acetylated samples were analyzed by Western blot with acetyl-lysine antibody. Acetylated samples were immunoprecipitated by acetyl-lysine antibody agarose (Immunechem) and further analyzed with anti-GOT2 antibody (Santa Cruz). GOT activity were measured using commercially available kit (Sigma).

Antibodies, Western blot and immunoprecipitation

Acetyl-lysine antibody (Cell Signaling), IDH3A (Abcam), PDHE1 (Abcam), OGDH (Abcam), CS, Uqcrc1, Uqcrb, Cox5b, GCN5L1, Sirt3 (Cell Signaling), VDAC1 (Santa Cruz), CypD (Abcam), OSCP (Abcam), Ndufs4 (Abcam), Ndufs3 (Abcam), Ndufb6 (Abcam), Ndufa9 (Abcam), SDHA (Abcam), ND1 (Abcam), ND2 (Abcam), ND3 (Abcam), ND4 (Abcam) and ND5 (Abcam). Cardiac tissues were homogenized with RIPA buffer (Sigma) using bullet blender at 4 °C for 10 minutes. Protein concentrations of supernatants were collected after centrifugation and quantified by Lowry assay. Protein lysates were loaded to 10 % SDS-PAGE, transferred to PVDF membrane and blocked with 5 % BSA in TSBT. Specific proteins were detected by specific antibodies listed above and corresponding secondary antibodies. Signals were visualized by HRP-derived chemiluminescence (Pierce) and film. Protein levels were quantified by Image-J.

In acetylation analysis, cardiac mitochondria were lysed with RIPA buffer and further diluted by IP buffer (50 mM MOPS pH 7.2, 10 mM Sodium phosphate, 50 mM Sodium chloride). IP buffer pre-washed acetyl-lysine antibody-conjugated agarose (Immunechem, Burnaby) was incubated with the cleared lysate at 4 °C overnight with mild agitation. Agarose bound with acetylated proteins was washed gently with IP buffer for three times by centrifugation. Bound acetylated proteins were released by SDS loading buffer and 5-minute heating at 95 °C. Samples were loaded to SDS-PAGE for analysis.

In co-immunoprecipitation of CypD or OSCP, isolated mitochondria were lysed with buffer containing detergent digitonin. Lysate were mixed with CypD (Abcam) antibodies. Antibodies bound proteins were precipitated with IgA/G agarose (Santa Cruz) and washed three times with lysis buffer. Samples were prepared with SDS-PAGE buffer and boiled for further analysis by Western blotting.

Statistical analysis

Comparisons among the multiple groups were performed by 1-way ANOVA, followed by Newman-Keuls multiple comparison test. For comparisons only involving two groups, unpaired 2-tailed t-tests were used. For repeated measurements of multiple groups, 2-way repeated measure ANOVA was performed. All analyses were performed using GraphPad Prism 6.0. All data are expressed as mean ± SEM and a $p<0.05$ was considered significant. All analyses were validated with permutation test versions, which are not dependent on any assumption of data distribution.

References

1.   Karamanlidis G, Lee CF, Garcia-Menendez L, Kolwicz SC, Jr., Suthammarak W, Gong G, Sedensky MM, Morgan PG, Wang W and Tian R. Mitochondrial complex I deficiency increases protein acetylation and accelerates heart failure. *Cell metabolism*. 2013;18:239-50.

2.   Hsu CP, Oka S, Shao D, Hariharan N and Sadoshima J. Nicotinamide phosphoribosyltransferase regulates cell survival through NAD+ synthesis in cardiac myocytes. *Circ Res*. 2009;105:481-91.

3.   Yan J, Young ME, Cui L, Lopaschuk GD, Liao R and Tian R. Increased glucose uptake and oxidation in mouse hearts prevent high fatty acid oxidation but cause cardiac dysfunction in diet-induced obesity. *Circulation*. 2009;119:2818-28.

4.   Kolwicz SC, Olson DP, Marney LC, Garcia-Menendez L, Synovec RE and Tian R. Cardiac-Specific Deletion of Acetyl CoA Carboxylase 2 (ACC2) Prevents Metabolic Remodeling During Pressure-Overload Hypertrophy. *Circ Res*. 2012;111:728-38.

5.   Boehm EA, Jones BE, Radda GK, Veech RL and Clarke K. Increased uncoupling proteins and decreased efficiency in palmitate-perfused hyperthyroid rat heart. *Am J Physiol Heart Circ Physiol*. 2001;280:H977-83.

6.   Keller A, Nesvizhskii AI, Kolker E and Aebersold R. Empirical statistical model to estimate the accuracy of peptide identifications made by MS/MS and database search. *Anal Chem*. 2002;74:5383-92.

7.   Nesvizhskii AI, Keller A, Kolker E and Aebersold R. A statistical model for identifying proteins by tandem mass spectrometry. *Anal Chem*. 2003;75:4646-58.

8.   Elias JE and Gygi SP. Target-decoy search strategy for increased confidence in large-scale protein identifications by mass spectrometry. *Nat Methods*. 2007;4:207-14.

9.   Ma K, Vitek O and Nesvizhskii AI. A statistical model-building perspective to identification of MS/MS spectra with PeptideProphet. *BMC Bioinformatics*. 2012;13 Suppl 16:S1.

10.   Liu H, Sadygov RG and Yates JR, 3rd. A model for random sampling and estimation of relative protein abundance in shotgun proteomics. *Anal Chem*. 2004;76:4193-201.

11.   Eng JK, Jahan TA and Hoopmann MR. Comet: an open-source MS/MS sequence database search tool. *Proteomics*. 2013;13:22-4.

12.   Valot B, Langella O, Nano E and Zivy M. MassChroQ: a versatile tool for mass spectrometry quantification. *Proteomics*. 2011;11:3572-7.

13.   Schneidman-Duhovny D, Inbar Y, Nussinov R and Wolfson HJ. PatchDock and SymmDock: servers for rigid and symmetric docking. *Nucleic Acids Res*. 2005;33:W363-7.

14.   Marcu R, Neeley CK, Karamanlidis G and Hawkins BJ. Multi-parameter measurement of the permeability transition pore opening in isolated mouse heart mitochondria. *Journal of visualized experiments : JoVE*. 2012;7,ppi:4131.

15.   Wiczer BM, Marcu R and Hawkins BJ. KB-R7943, a plasma membrane Na(+)/Ca(2+) exchanger inhibitor, blocks opening of the mitochondrial permeability transition pore. *Biochem Biophys Res Commun*. 2014;444:44-9.

16.   Scholz TD and Koppenhafer SL. Reducing equivalent shuttles in developing porcine myocardium: enhanced capacity in the newborn heart. *Pediatr Res*. 1995;38:221-7.

17.   Wagner GR and Payne RM. Widespread and enzyme-independent Nepsilon-acetylation and Nepsilon-succinylation of proteins in the chemical conditions of the mitochondrial matrix. *The Journal of biological chemistry*. 2013;288:29036-45.

Supplementary Table 1: clinical data of the human subjects. ICM: ischemic cardiomyopathy. DCM: dilated cardiomyopathy. BMI: body mass index. EF: ejection fraction.

Groups	N	Age	BMI	EF (%)	ICM/DCM ratio
Non-failing	8	58±5	N/A	N/A	N/A
Failing	10	54±9	27±2.8	15.6±2.5	1:1

Supplementary Table 2: List of C-I proteins showed significant changes in levels from mitochondrial proteome analysis (cKO/Con > 2 or < 0.5; P<0.01, n=4).

IPI ID	Protein name	cKO/Con
IPI00169925	Ndufv2	0.50
IPI00230715	Ndufa13	0.50
IPI00133215	Ndufb7	0.49
IPI00944067	Ndufa9	0.48
IPI00318645	Ndufa11	0.48
IPI00128023	Ndufs2	0.47
IPI00132531	Ndufb5	0.47
IPI00403381	Ndufv3	0.45
IPI00132940	Ndufa1	0.44
IPI00116748	Ndufa10	0.44
IPI00341550	ND1	0.44
IPI00114246	Ndufb11	0.44
IPI00930784	Ndufs1	0.42
IPI00341322	Ndufb6	0.40
IPI00130460	Ndufv1	0.40
IPI00117300	Ndufs5	0.32
IPI00387430	Ndufb8	0.32
IPI00133399	Ndufa6	0.30
IPI00132050	Ndufc2	0.23
IPI00131994	Ndufb2	0.22
IPI00130322	Ndufa7	0.20
IPI00344004	Ndufa12	0.20
IPI00229008	Ndufs4	0.14

Supplementary Table 3: list of cardiac mitochondrial proteins identified and spectral count values

	Con-1	Con-2	Con-3	Con-4	cKO-1	cKO-2	cKO-3	cKO-4	Ave-Con	Ave-cKO	P-value
IPI00108410	8	8	6	3	7	6	5	3	6.3	5.3	0.52
IPI00109109	46	46	49	43	51	42	52	51	46.0	49.0	0.30
IPI00109169	58	50	56	60	50	57	56	57	56.0	55.0	0.73
IPI00109501	3	5	5	4	3	3	6	4	4.3	4.0	0.78
IPI00109611	5	4	7	7	5	3	5	6	5.8	4.8	0.35
IPI00109655	6	4	3	3	2	6	5	5	4.0	4.5	0.67
IPI00110385	8	9	5	9	7	9	9	9	7.8	8.5	0.51
IPI00110578	2		2	2	1	2	2	3	2.0	2.0	1.00
IPI00111211	3	4	3	5	3	4	4	2	3.8	3.3	0.49
IPI00111885	167	187	208	218	204	209	189	198	195.0	200.0	0.69
IPI00112032	4	6	5	6	3	2	9	6	5.3	5.0	0.88
IPI00112986	3	4	3	3	2	3	3	2	3.3	2.5	0.10
IPI00113073	3		4	2	4	6	3	4	3.0	4.3	0.22
IPI00113143	16	15	16	15	14	21	13	10	15.5	14.5	0.68
IPI00113196	17	14	14	9	15	15	15	13	13.5	14.5	0.58
IPI00113386	3	2	2	6	4	4	6	6	3.3	5.0	0.17
IPI00113517	7	7	4	7	5	9	6	6	6.3	6.5	0.83
IPI00113606	2	3	2	4	5	5	1	3	2.8	3.5	0.51
IPI00114246	24	34	27	25	12	14	10	12	27.5	12.0	0.00
IPI00114331	5	4	2	3	2	4	3	1	3.5	2.5	0.32
IPI00114342	3	6	5	4	5	7	5	6	4.5	5.8	0.17
IPI00114377	18	27	16	18	29	27	22	17	19.8	23.8	0.31
IPI00114710	12	9	13	12	11	12	9	9	11.5	10.3	0.32
IPI00114840	3	3	5	3	5	4	7	4	3.5	5.0	0.13
IPI00115598	3	3	4	4	5	6	7	6	3.5	6.0	0.00
IPI00115896	3	3	2	2	3	3	2	3	2.5	2.8	0.54
IPI00115949	3	4	8	8	8	8	11	10	5.8	9.3	0.06
IPI00116074	470	503	491	462	517	537	504	519	481.5	519.3	0.02
IPI00116154	69	79	73	75	77	81	74	74	74.0	76.5	0.38
IPI00116169	5	7	5	3	2	3	4	2	5.0	2.8	0.05

IPI00116192	41	41	39	39	38	33	42	47	40.0	40.0	1.00
IPI00116222	16	18	24	21	43	35	39	52	19.8	42.3	0.00
IPI00116748	74	77	82	86	43	40	26	32	79.8	35.3	0.00
IPI00116843	47	52	51	52	31	34	26	31	50.5	30.5	0.00
IPI00116896	6	7	7	8	9	9	8	6	7.0	8.0	0.27
IPI00117083	6	4		3	3	3	2	3	4.3	2.8	0.10
IPI00117300	13	10	12	15	6	4	3	3	12.5	4.0	0.00
IPI00117312	119	119	121	116	131	140	128	137	118.8	134.0	0.00
IPI00118316	5	4	17	15	2	4	5	4	10.3	3.8	0.11
IPI00118963	19	14	5	3	16	8	16	12	10.3	13.0	0.54
IPI00119114	163	170	166	157	182		199	197	164.0	192.7	0.00
IPI00119138	233	266	322	349	428	422	398	327	292.5	393.8	0.03
IPI00119576	2	2	2	3	2	3	5	4	2.3	3.5	0.12
IPI00119945	5	7	6	6	8	5	3	5	6.0	5.3	0.52
IPI00120232	23	24	26	27	17	16	12	20	25.0	16.3	0.00
IPI00120233	4	5	6	3	6	4	3	4	4.5	4.3	0.79
IPI00120414	8	8	10	7	11	6		12	8.3	9.7	0.45
IPI00120671	4	4	4	5	4	5	6	5	4.3	5.0	0.17
IPI00120719	78	87	87	69	83	82	88	93	80.3	86.5	0.26
IPI00120984	12	19	6	11	8	5	6	7	12.0	6.5	0.09
IPI00121051	17	19	17	18	21	15	18	18	17.8	18.0	0.86
IPI00121105	153	146	143	146	170	168	161	166	147.0	166.3	0.00
IPI00121218	7	5	7	6	7	5	7	9	6.3	7.0	0.46
IPI00121443	6	3	5	5	10	6	12	6	4.8	8.5	0.06
IPI00121576	19	19	13	14	21	24	21	18	16.3	21.0	0.06
IPI00122251	14	10	9	6	9	6	8	7	9.8	7.5	0.25
IPI00122740	15	15	15	17	18	13	11	15	15.5	14.3	0.46
IPI00123765	2	4	3	4	4	4	4	4	3.3	4.0	0.17
IPI00124067	2	3				1			2.5	1.0	N/A
IPI00124771	112	126	129	138	121	120	138	143	126.3	130.5	0.61
IPI00125592	4	5	5	6	5	2	3	3	5.0	3.3	0.06
IPI00125929	22	25	25	28	21	22	28	29	25.0	25.0	1.00

IPI00126120	3	3	5	4	3	4	4	4	3.8	3.8	1.00
IPI00126635	66	61	86	74	79	71	77	71	71.8	74.5	0.65
IPI00126913	4	5	5	5	7	4	6	7	4.8	6.0	0.15
IPI00127558	3	4		4				3	3.7	3.0	N/A
IPI00128201	2	3	2	1		3	4	2	2.0	3.0	0.20
IPI00128346	18	21	18	15	19	18	20	25	18.0	20.5	0.25
IPI00129178	14	18	17	14	22	19	19	19	15.8	19.8	0.02
IPI00129516	12	8	11	8	9	8	11	10	9.8	9.5	0.84
IPI00129577	26	26	27	25	37	33	28	32	26.0	32.5	0.01
IPI00130322	11	11	11	16	2	3			12.3	2.5	0.01
IPI00130331	4	1	5	5	4	5	5	2	3.8	4.0	0.84
IPI00130376	20	19					21	17	19.5	19.0	0.83
IPI00130530	2	2		1		3			1.7	3.0	N/A
IPI00130535	13			13	15	14			13.0	14.5	0.10
IPI00131176	135	147	144	147	157	159	159	161	143.3	159.0	0.00
IPI00131584	41	42	35	37	39	31	32	34	38.8	34.0	0.10
IPI00131695	6	6	6	7	2	4	6	8	6.3	5.0	0.38
IPI00132002	10	14	19	13	14	22	15	18	14.0	17.3	0.26
IPI00132042	101	104	119	123	123	131	122	130	111.8	126.5	0.05
IPI00132217	3	3	3	2	2	2		2	2.8	2.0	0.05
IPI00132412	3	4	3	2	4	5	2	5	3.0	4.0	0.27
IPI00132478	3	6	3	2	4	3	3	2	3.5	3.0	0.62
IPI00132623	48	38	49	48	23	29	25	21	45.8	24.5	0.00
IPI00132696	4	2	4	2	3	4	3	4	3.0	3.5	0.47
IPI00132762	10	17	17	15	17	15	21	10	14.8	15.8	0.74
IPI00132940	4	4	6	4		2	2	2	4.5	2.0	0.01
IPI00132958	71	49	57	54	57	60	59	62	57.8	59.5	0.73
IPI00133006	26	24	24	23	21	17	18	16	24.3	18.0	0.00
IPI00133015	3	3	3	3	5	4	6	5	3.0	5.0	0.00
IPI00133034	10	10	14	13	9	13	7	11	11.8	10.0	0.33
IPI00133215	40	38	36	38	21	23	17	14	38.0	18.8	0.00
IPI00133240	62	58	65	57	65	67	66	56	60.5	63.5	0.38

IPI00133270	3	3	6	5	3	5	5	4	4.3	4.3	1.00
IPI00133392	7	10	46	29	9	11	18	17	23.0	13.8	0.36
IPI00133399	7	10	8	8	3	2	3	2	8.3	2.5	0.00
IPI00133403	5	5	7	8	4	2	5	3	6.3	3.5	0.03
IPI00133411	3	2	4	3	5	1	5	4	3.0	3.8	0.49
IPI00133608	5	4	7	7	4	4	9	6	5.8	5.8	1.00
IPI00133776	2	3	4	4	2	2	2	7	3.3	3.3	1.00
IPI00133778	2	2	2	1	1	3	2		1.8	2.0	0.68
IPI00133903	69	73	71	68	74	82		80	70.3	78.7	0.02
IPI00134484	2	2	3	4	4	4	3	4	2.8	3.8	0.11
IPI00134572	2	3	3	3	3	3	3	2	2.8	2.8	1.00
IPI00134918	3	1		1		2			1.7	2.0	N/A
IPI00135068	8	6	6	7	5	6	7	7	6.8	6.3	0.49
IPI00135446	2		1	3	3	4	1	1	2.0	2.3	0.81
IPI00135651	73	85	75	72	78	85	71	84	76.3	79.5	0.49
IPI00136201	4	4	2	4	3	4	2	6	3.5	3.8	0.81
IPI00136563	74	76	70	68	85	90	89	84	72.0	87.0	0.00
IPI00137424	4	4	6	7	10	9	9	5	5.3	8.3	0.07
IPI00137601	4	5	6	7	7	6	7	9	5.5	7.3	0.10
IPI00153660	72	71	61	55	79	80	61	69	64.8	72.3	0.26
IPI00153792	15	18	17	20	12	23	13	18	17.5	16.5	0.73
IPI00154054	86	91	96	88	83	92	80	88	90.3	85.8	0.24
IPI00162942	2	2	2	2	2	4	2	2	2.0	2.5	0.36
IPI00170093	28	27	23	25	17	16	14	16	25.8	15.8	0.00
IPI00170126	5	6	6	7	4	8	6	9	6.0	6.8	0.55
IPI00170307	2	6	4	4	6	5	7	6	4.0	6.0	0.07
IPI00221407	9	8	10	5	10	8	7	8	8.0	8.3	0.85
IPI00221569	6	10	3	4	8	7	11	12	5.8	9.5	0.10
IPI00221608	23	24	25	26	26	26	27	31	24.5	27.5	0.07
IPI00221782	10	9	10	14	12	12	12	13	10.8	12.3	0.24
IPI00223092	752	766	742	824	924	930	853	730	771.0	859.3	0.13
IPI00224210	12	12	18	14	8	11	10	11	14.0	10.0	0.04

IPI00225390	61	63	67	60	60	63	69	73	62.8	66.3	0.33
IPI00226140	14	16	17	13	16	19	16	10	15.0	15.3	0.91
IPI00226521	11	11	8	4	9	8	7	8	8.5	8.0	0.78
IPI00227186	4	2	4	3	2		1	1	3.3	1.3	0.03
IPI00228106	2		4	3	4	4	6	4	3.0	4.5	0.11
IPI00228343	2	2	3	3	2	1	2	5	2.5	2.5	1.00
IPI00229008	21	20	24	19	2	4	4	2	21.0	3.0	0.00
IPI00230351	204	214	249	236	220	219	206	210	225.8	213.8	0.31
IPI00230715	52	53	51	59	30	26	24	27	53.8	26.8	0.00
IPI00261627	81	82	125	138	127	146	140	129	106.5	135.5	0.11
IPI00271986	33	34	37	37	45	43	29	40	35.3	39.3	0.32
IPI00273164	9	10	11	9	8	9	9	11	9.8	9.3	0.55
IPI00274222	6	11	9	13	10	10	11	8	9.8	9.8	1.00
IPI00274656	7	3	2		3	3		3	4.0	3.0	0.55
IPI00308162	84	91	81	80	89	88	92	84	84.0	88.3	0.20
IPI00312174	8	10	9	8	6	6	7	7	8.8	6.5	0.01
IPI00312507	5	6	4	2	3	2	1	2	4.3	2.0	0.05
IPI00312720	3	1	1	1	2	2	3	1	1.5	2.0	0.47
IPI00315135	6	5	6	4	6	4	4	5	5.3	4.8	0.49
IPI00315302	8	10	9	9	6	6	3	5	9.0	5.0	0.00
IPI00315325	2			3	2	2	2	2	2.5	2.0	0.18
IPI00315808	12	11	11	9	14	14	15	15	10.8	14.5	0.00
IPI00315908	13	17	15	12	16	20	12	13	14.3	15.3	0.65
IPI00317989	5	2			2	2	7	4	3.5	3.8	0.91
IPI00318935	3	2	2	3	2		2		2.5	2.0	0.31
IPI00319111	10	11	13	16	11	12	10	11	12.5	11.0	0.32
IPI00319518	32	35	38	38	44	47	46	46	35.8	45.8	0.00
IPI00320238	9	13	10	10	13	14	11	14	10.5	13.0	0.07
IPI00320503	3	6	9	4	7	7	4	5	5.5	5.8	0.87
IPI00321617	4	7	4	5	5	3	6	6	5.0	5.0	1.00
IPI00323592	206	202	202	195	216	228	223	240	201.3	226.8	0.00
IPI00331182	3	2	4	5	3	3	2	5	3.5	3.3	0.79

IPI00331214	3	4	5	3	3	1	2	4	3.8	2.5	0.17
IPI00331436	4	6	3		8	2	6	7	4.3	5.8	0.45
IPI00331555	16	18	13	16	18	19	20	20	15.8	19.3	0.02
IPI00337893	89	93	84	96	96	100	84	87	90.5	91.8	0.79
IPI00338536	59	62	59	56	60	69	54	49	59.0	58.0	0.83
IPI00341282	122	132	122	124	159	151	152	132	125.0	148.5	0.01
IPI00341322	13	19	15	20	9	6	5	7	16.8	6.8	0.00
IPI00341550	23	21	21	22	10	10	7	11	21.8	9.5	0.00
IPI00378120	2	3	5	1	2	3	4	6	2.8	3.8	0.44
IPI00380273	3	1	1	2	1	1	1	2	1.8	1.3	0.39
IPI00387379	104	107	93	87	104	94	113	107	97.8	104.5	0.31
IPI00387430	30	35	41	38	14	13	10	9	36.0	11.5	0.00
IPI00406442	72	79	85	66	82	98	103	71	75.5	88.5	0.17
IPI00459487	17	22	19	20	22	19	16	14	19.5	17.8	0.42
IPI00461964	56	56	63	66	56	66	55	63	60.3	60.0	0.95
IPI00467124	7	3	5	3	5	5	5	4	4.5	4.8	0.81
IPI00468481	2608	2723	2526	2147	2736	2472	2831	2643	2501.0	2670.5	0.29
IPI00469942	42	48	52	58	45	43	34	30	50.0	38.0	0.05
IPI00471246	70	85	78	84	85	89	75	81	79.3	82.5	0.50
IPI00480233	22	21	25	21	19	19	5	6	22.3	12.3	0.05
IPI00604945	2	3	2	2	2	2	2	3	2.3	2.3	1.00
IPI00624653	4	6	4	5	4	3	5	5	4.8	4.3	0.49
IPI00626928	6	4	4	3	5	3	3	4	4.3	3.8	0.55
IPI00672663	3	2	4	3	3	2			3.0	2.5	0.51
IPI00755181	2	3				1			2.5	1.0	N/A
IPI00757372	43	42	44	37	47	49	47	49	41.5	48.0	0.01
IPI00762636	4	4	7	5	6	6	4	1	5.0	4.3	0.61
IPI00109275	2	3	6	3	2	4	3	1	3.5	2.5	0.39
IPI00110658	10	4	10	9	7	8	10	5	8.3	7.5	0.69
IPI00110721	4	4	6	8	6	4	6	7	5.5	5.8	0.83
IPI00110850	6								6.0	N/A	N/A
IPI00111013	14	15	13	13	15	10	7	13	13.8	11.3	0.22

IPI00111218	54	65	55	54	49	52	44	44	57.0	47.3	0.03
IPI00111770	34	33	34	28	36	38	32	27	32.3	33.3	0.74
IPI00112493	10	13	11	10	13	8	10	11	11.0	10.5	0.70
IPI00112549	105	112	107	93	115	105	117	121	104.3	114.5	0.10
IPI00113052	6	7	8	8	12	10	9	11	7.3	10.5	0.01
IPI00113141	140	167	164	157	172	167	157	172	157.0	167.0	0.20
IPI00113347	60	61	51		58	52		53	57.3	54.3	0.46
IPI00114209	34	26	28	30	26	25	25	29	29.5	26.3	0.15
IPI00114866	11	12	9	11	14	8	7	12	10.8	10.3	0.79
IPI00115094	5	8	10	14	6	10	8	7	9.3	7.8	0.50
IPI00115459	4	4	4	3	4	6	3	2	3.8	3.8	1.00
IPI00115564	731	794	897	915	872	902	903	919	834.3	899.0	0.20
IPI00115607	1037	1098	1002	1022	1076	1083	1057	1047	1039.8	1065.8	0.29
IPI00116228	11	16	16	16	15	15	21	15	14.8	16.5	0.40
IPI00116753	219	216	235	213	227	240	241	248	220.8	239.0	0.03
IPI00117214	35	37	29	30	37	41	39	39	32.8	39.0	0.02
IPI00117281	3	4	3	4	4	6	3	4	3.5	4.3	0.32
IPI00117657	27	26	26	30	29	28	27	34	27.3	29.5	0.26
IPI00117978	88	89	92	89	83	92	95	108	89.5	94.5	0.38
IPI00118986	90	97	101	99	105	111	104	106	96.8	106.5	0.01
IPI00119203	217	240	225	216	172	165	141	174	224.5	163.0	0.00
IPI00119842	27	26	26	24	24	25	22	22	25.8	23.3	0.04
IPI00120076	723	712	754	810	960	966	962	870	749.8	939.5	0.00
IPI00120199	10	11	7	6	10	13	7	6	8.5	9.0	0.81
IPI00121276	10	2	5	8	14	10	10	12	6.3	11.5	0.04
IPI00121288	36	44	42	36	23	18	21	23	39.5	21.3	0.00
IPI00121309	48	46	41	40	29	29	31	27	43.8	29.0	0.00
IPI00121322	114	101	87	77	101	105	130	110	94.8	111.5	0.16
IPI00121440	115	116	100	96	92	93	96	95	106.8	94.0	0.05
IPI00122442	30	32	21	23	30	37	23	28	26.5	29.5	0.47
IPI00122499	7	9	13	10	8	9	9	5	9.8	7.8	0.25
IPI00122547	31	35	36	35	39	37	47	46	34.3	42.3	0.03

IPI00122548	41	47	53	51	65	64	67	78	48.0	68.5	0.00
IPI00122549	120	123	120	130	133	137	156	166	123.3	148.0	0.02
IPI00122554	38	33	33	34	31	28	29	24	34.5	28.0	0.01
IPI00122633	5	4	6	5	11	9	8	8	5.0	9.0	0.00
IPI00123316	6	4	11	9		1	2	1	7.5	1.3	0.02
IPI00124292	9	11	10	9	12	14	14	9	9.8	12.3	0.10
IPI00124699	4	4	3	2	3	2	2	3	3.3	2.5	0.23
IPI00124900	7	10	8	8	10	10	11	10	8.3	10.3	0.03
IPI00125035	5	1	2						2.7 N/A		N/A
IPI00125460	32	31	39	39	38	43	32	41	35.3	38.5	0.35
IPI00125776	3	5	2	3	3	4	3		3.3	3.3	0.92
IPI00127050	14	15	16	18	18	20	17	13	15.8	17.0	0.49
IPI00127227	7	8	9	8	9	10	8	9	8.0	9.0	0.13
IPI00128023	129	130	122	122	67	60	59	52	125.8	59.5	0.00
IPI00128345	18	12	13	14	8	9	4	9	14.3	7.5	0.01
IPI00128642	11	10	7	8	16	15	11	7	9.0	12.3	0.20
IPI00129164	2	2	2	2	2	3	2	3	2.0	2.5	0.13
IPI00129404	58	60	265	251	33	38	95	90	158.5	64.0	0.17
IPI00129517	41	40	42	38	41	45	37	48	40.3	42.8	0.36
IPI00130018	3				1	2	3	3	3.0	2.3 N/A	
IPI00130280	997	1024	998	1013	1070	1066	1106	1066	1008.0	1077.0	0.00
IPI00130460	123	104	134	120	52	53	44	44	120.3	48.3	0.00
IPI00130733	3	3	2	3	3	4	7	6	2.8	5.0	0.05
IPI00130804	66	57	64	52	59	53	51	46	59.8	52.3	0.12
IPI00131177	14	18	19	15	15	12	10	12	16.5	12.3	0.04
IPI00131771	29	38	42	38	37	40	50	41	36.8	42.0	0.23
IPI00131896	35	36	30	27	31	25	30	36	32.0	30.5	0.65
IPI00132039	13	9	21	16	18	15	16	17	14.8	16.5	0.53
IPI00132050	15	17	17	12		4		3	15.3	3.5	0.00
IPI00132347	66	65	62	59	64	70	60	62	63.0	64.0	0.72
IPI00132390	17	23	22	20	15	16	7	10	20.5	12.0	0.01
IPI00132531	22	24	28	24	12	11	12	11	24.5	11.5	0.00

IPI00132653	116	125	143	132	133	127	155	121	129.0	134.0	0.61
IPI00132728	108	115	105	122	133	135	117	116	112.5	125.3	0.09
IPI00132799	28	22	27	20	24	24	31	33	24.3	28.0	0.26
IPI00132895	2		2	3	4	3			2.3	3.5	0.13
IPI00133284	86	99	68	64	117	115	125	127	79.3	121.0	0.00
IPI00133440	30	36	29	35	38	39	34	39	32.5	37.5	0.06
IPI00133562	24	27	24	23	26	20	21	16	24.5	20.8	0.14
IPI00134809	53	52	49	54	60	69	76	72	52.0	69.3	0.00
IPI00134961	123	134	139	129	155	152	127	138	131.3	143.0	0.16
IPI00136333	4	3	5	4	2	4	5	3	4.0	3.5	0.54
IPI00136683	48	48	45	43	61	55	52	50	46.0	54.5	0.02
IPI00153266	11	8	12	12	14	12	6	9	10.8	10.3	0.81
IPI00153381	11	15	10	12	11	12	12	14	12.0	12.3	0.85
IPI00153903	19	20	19	22	23	22	21	17	20.0	20.8	0.63
IPI00154047	28	31	33	40	34	37	40	45	33.0	39.0	0.13
IPI00169752	4		6	3	4	4	3	2	4.3	3.3	0.30
IPI00169862	22	29	20	29	18	29	21	28	25.0	24.0	0.79
IPI00169925	50	55	59	50	19	33	27	28	53.5	26.8	0.00
IPI00170213	8	8	3	6	4	8	13	9	6.3	8.5	0.34
IPI00170357	11	10	11	10	13	11	8	16	10.5	12.0	0.41
IPI00221769	12	9	12	16	10	8	13	14	12.3	11.3	0.63
IPI00222284	6	6	6	6	6	4	4	4	6.0	4.5	0.02
IPI00222419	29	37	39	38	39	36	40	41	35.8	39.0	0.25
IPI00222526	8	8	8	8	4	2	3	3	8.0	3.0	0.00
IPI00222767	24	22	24	24	19	30	23	25	23.5	24.3	0.76
IPI00223216	5	7	7	5	7	6	3	5	6.0	5.3	0.49
IPI00225254	28	35	39	30	32	37	25	28	33.0	30.5	0.51
IPI00226466	5	2	2	3	2	5	3	4	3.0	3.5	0.62
IPI00228150	96	90	105	103	114	110	109	91	98.5	106.0	0.27
IPI00230283	8	4	6	4	9	6	4	6	5.5	6.3	0.61
IPI00230507	116	113	120	122	123	135	119	124	117.8	125.3	0.11
IPI00230754	103	105	82	89	112	103	108	109	94.8	108.0	0.06

IPI00263863	10	10	12	9	11	10	9	10	10.3	10.0	0.75
IPI00267983	25	25	30	30	27	29	31	30	27.5	29.3	0.34
IPI00269076	8	8	9	10	7	11	18	11	8.8	11.8	0.25
IPI00274407	46	53	54	58	60	56	49	54	52.8	54.8	0.58
IPI00278230	5	5	5	6	6	6	5	4	5.3	5.3	1.00
IPI00283203	3				3	2			3.0	2.5	N/A
IPI00308885	154	166	140	160	192	186	211	202	155.0	197.8	0.00
IPI00311072	4	7	4	3	7	6	5	2	4.5	5.0	0.73
IPI00313998	10	11	9	8	11	10	12	5	9.5	9.5	1.00
IPI00318283	4	3	5	3	3	3	5	4	3.8	3.8	1.00
IPI00318614	403	423	464	385	564	529	553	453	418.8	524.8	0.01
IPI00318645	27	24	30	28	13	15	12	12	27.3	13.0	0.00
IPI00318750	11	16	7	12	9	12	14	11	11.5	11.5	1.00
IPI00320462	6	5	4	5	5	5	7	5	5.0	5.5	0.47
IPI00320716	14	12	11	8	12	12	10	6	11.3	10.0	0.53
IPI00320850	32	41	33	35	36	37	33	38	35.3	36.0	0.75
IPI00321718	25	32	26	21	29	27	31	28	26.0	28.8	0.30
IPI00322931	20	21	21	21	23	21	18	24	20.8	21.5	0.60
IPI00323357	4	2	2	2	3	3		2	2.5	2.7	0.81
IPI00330523	41				37	34			41.0	35.5	N/A
IPI00331251	81	81	90	73	93	85	100	107	81.3	96.3	0.04
IPI00331332	43	53	46	54	26	27	27	28	49.0	27.0	0.00
IPI00331692	102	100	86	77	125	114	107	108	91.3	113.5	0.02
IPI00338964	16	18	17	15	12	9	9	14	16.5	11.0	0.01
IPI00344004	42	53	54	60	12	14	9	6	52.3	10.3	0.00
IPI00347110	3	3		1			1	1	2.3	1.0	0.22
IPI00379694	9	11	9	6	6	13		10	8.8	9.7	0.68
IPI00379695	11	10	11	9	10	12	10	8	10.3	10.0	0.80
IPI00403381	9	7	6	7	3	3	4	3	7.3	3.3	0.00
IPI00408243	7	8	3	5	4	3	6	7	5.8	5.0	0.62
IPI00420706	58	59	77	60	83	76	72	69	63.5	75.0	0.08
IPI00453499	29	30	33	31	46	42	33	30	30.8	37.8	0.12

IPI00453777	301	296	152	81	313	137	459	283	207.5	298.0	0.33
IPI00454049	52	57	48	45	60	52	49	52	50.5	53.3	0.46
IPI00454201	9	11	13	13	15	10	13	11	11.5	12.3	0.63
IPI00459383	6	8	11	9	6	9	12	6	8.5	8.3	0.89
IPI00459725	175	175	168	192	168	169	196	183	177.5	179.0	0.86
IPI00468850	12	8	13	8	18	13	15	18	10.3	16.0	0.02
IPI00469195	7	7	3		2	3		1	5.7	2.0	0.07
IPI00474157	7	9	7	6	8	7	5	10	7.3	7.5	0.84
IPI00553333	7	6			7	10			6.5	8.5	0.33
IPI00553717	48	47	48	43	44	45	45	38	46.5	43.0	0.14
IPI00555015	5	5	25	20	4	5	7	6	13.8	5.5	0.16
IPI00626237	207	195	170	191	215	202	218	216	190.8	212.8	0.04
IPI00651782	62	69	56	53	66	58	58	53	60.0	58.8	0.79
IPI00653158	662	726	605	586	752	738	747	724	644.8	740.3	0.02
IPI00661338	10	14	11	13	11	9	8	12	12.0	10.0	0.17
IPI00672367	11	11	10	6	9	9	12	5	9.5	8.8	0.70
IPI00759881	13	12	14			17	23	17	13.0	19.0	0.04
IPI00759940	191	222	208	268	234	245	274	208	222.3	240.3	0.43
IPI00762858	14		18	17	21	19	18	17	16.3	18.8	0.15
IPI00776084	72	77	81	73	71	78	81	81	75.8	77.8	0.55
IPI00785281	4								4.0 N/A		N/A
IPI00798614	3	4	2	2	2		3	3	2.8	2.7	0.90
IPI00830581	40	45	54	56	51	48	47	51	48.8	49.3	0.90
IPI00850133	25	28	21	23	42	34	40	35	24.3	37.8	0.00
IPI00850737	29	22	31	32	20	22	23	22	28.5	21.8	0.03
IPI00874456	266	274	276	272	299	281	301	282	272.0	290.8	0.02
IPI00876208	23	27	22	20	19	15	16		23.0	16.7	0.03
IPI00876323	12	17	14	18	10	14	10	16	15.3	12.5	0.23
IPI00881401	67	73	61	69	65		53		67.5	59.0	0.18
IPI00890322	61	60	69	69	59	52	52	50	64.8	53.3	0.01
IPI00918862	28	30			29	32	23	35	29.0	29.8	0.86
IPI00928176	26	25	23	25	27	22	17	15	24.8	20.3	0.15

ID	1	2	3	4	5	6	7	8	Avg1	Avg2	p
IPI00930784	169	176	173	176	77	72	65	78	173.5	73.0	0.00
IPI00944067	70	77	88	82	41	45	31	35	79.3	38.0	0.00
IPI00127417	4	3	3		2	3	1	5	3.3	2.8	0.60
IPI00132216	4	3	5						4.0	N/A	N/A
IPI00222538	2	2			2	3	2	3	2.0	2.5	0.31
IPI00269240	2	5	4	2	2		6	5	3.3	4.3	0.46
IPI00308195	2	7	5	4	6	5	5	6	4.5	5.5	0.39
IPI00321499	3	3	3		5	4	3	3	3.0	3.8	0.24
IPI00462749	2	2	2	2	4	4	2	2	2.0	3.0	0.13
IPI00125652	2			2	2	4			2.0	3.0	0.42
IPI00132954	2								2.0	N/A	N/A
IPI00224955	2	1	3		2		1	1	2.0	1.3	0.37
IPI00311682	2	2	2	2			2	2	2.0	2.0	N/A
IPI00318671	3		1	2	1		1	2	2.0	1.3	0.37
IPI00473646	2			3					2.5	N/A	N/A
IPI00119431	2	1	1		3	2	3	3	1.3	2.8	0.02
IPI00122687	2				1				2.0	1.0	N/A
IPI00129163	2			1			3		1.5	3.0	N/A
IPI00230760	2	3	6	7	2	3	2	4	4.5	2.8	0.22
IPI00454008	3	3	2	2	6	3	2	1	2.5	3.0	0.67
IPI00121833	4	5	3	2	3	4	4	2	3.5	3.3	0.77
IPI00153400	3	4							3.5	N/A	N/A
IPI00387249	3	3	3	3	1	3		3	3.0	2.3	0.29
IPI00453815	2					2	2		2.0	2.0	N/A
IPI00136310	2	2	2	3	2	3	3		2.3	2.7	0.35
IPI00227445	2			2	2		2	2	2.0	2.0	N/A
IPI00318901	2	1	4						2.3	N/A	N/A
IPI00421081	2	1	1	2	2	1	1	1	1.5	1.3	0.54
IPI00856534	10	11			11	12	14	15	10.5	13.0	0.15
IPI00131988	2	1	1	1	2	2	2	1	1.3	1.8	0.21
IPI00228548	2	5	2	3	6	4	1	2	3.0	3.3	0.86
IPI00318006	2	4	3	3	5	2	4	3	3.0	3.5	0.54

ID	C1	C2	C3	C4	C5	C6	C7	C8			
IPI00396833	2		2	2					2.0	N/A	N/A
IPI00133167	2			2		1	2	2	2.0	1.7	0.50
IPI00225747	2	2	1	2	4	2	4	2	1.8	3.0	0.09
IPI00896595	2	2	1	2	3	3		4	1.8	3.3	0.01
IPI00169883	3		3			4	2		3.0	3.0	1.00
IPI00133744	2	3	4	5	4	4	4	5	3.5	4.3	0.32
IPI00312058	2	1	5	6	2				3.5	2.0	N/A
IPI00314069	2		3		2	2		3	2.5	2.3	0.79
IPI00119846	2	4		2	3	3	4	2	2.7	3.0	0.67
IPI00135311	2	3	1		2	3	2	2	2.0	2.3	0.68
IPI00330551	2	4	2		7	5	7	5	2.7	6.0	0.01
IPI00624175	2	1	2	2	1	1	2	2	1.8	1.5	0.54
IPI00271726	2	2	1	3	3	5	2		2.0	3.3	0.19
IPI00319994	2	1							1.5	N/A	N/A
IPI00275050	2			3	3		2	2	2.5	2.3	0.79
IPI00112822	2	2	2	4	3	4	3	4	2.5	3.5	0.13
IPI00121641	2	2	3	3					2.5	N/A	N/A
IPI00137173	2		2	7	3	2	3		3.7	2.7	0.59
IPI00651954	3	2	4	3	2	5	2	5	3.0	3.5	0.62
IPI00378520	2	2	2			1			2.0	1.0	N/A
IPI00471097	2	2	2	2	2	2			2.0	2.0	N/A
IPI00187452	2								2.0	N/A	N/A
IPI00329998	2	3		2					2.3	N/A	N/A
IPI00118594	4	2		5	4	4	2		3.7	3.3	0.78
IPI00123096	4	5	6	4	4	4	6	5	4.8	4.8	1.00
IPI00222096	3								3.0	N/A	N/A
IPI00121834	2	2	4		5	2			2.7	3.5	0.60
IPI00464317	2	3					3	3	2.5	3.0	0.42
IPI00138406	2					1			2.0	1.0	N/A
IPI00622235	3								3.0	N/A	N/A
IPI00222409	2								2.0	N/A	N/A
IPI00226024	2								2.0	N/A	N/A

	1	2	3	4	5	6	7	8			
IPI00331442	2	2	5	3	2		3		3.0	2.5	0.67
IPI00817011	2								2.0	N/A	N/A
IPI00109354	1	1	1	1	1	1	1	3	1.0	1.5	0.36
IPI00112126	2	1	1	2		1		2	1.5	1.5	1.00
IPI00114153	1	2		4	1		2	3	2.3	2.0	0.77
IPI00114378	3	5	10	10	5		5	3	7.0	4.3	0.28
IPI00116170	5	3	4	4	3	3	3	3	4.0	3.0	0.05
IPI00131994	11	8	10	7	3	2	1		9.0	2.0	0.00
IPI00135579	2	3	3	3	2	2	4	4	2.8	3.0	0.70
IPI00262198	2	4	1		2		5	1	2.3	2.7	0.83
IPI00331490	1	2	2	1	1	1	2	2	1.5	1.5	1.00
IPI00355268	1	2	1	2	1				1.5	1.0	N/A
IPI00421284	1	1	1	1	1	1	1	1	1.0	1.0	N/A
IPI00672824	1	1	1	1	1	1	1	1	1.0	1.0	N/A
IPI00460669	1								1.0	N/A	N/A
IPI00109740	1	2		1	3	1	2		1.3	2.0	0.37
IPI00113080	1	2	1						1.3	N/A	N/A
IPI00115117	1	1	1	2	1	1			1.3	1.0	0.54
IPI00130102	1	1	1	1			1	1	1.0	1.0	N/A
IPI00132148	5	6	5	5	4	3	5	6	5.3	4.5	0.32
IPI00132504	1	1				2	2	3	1.0	2.3	0.05
IPI00169953	1	1	1	2	1	1	1	1	1.3	1.0	0.36
IPI00223197	2	1	1						1.3	N/A	N/A
IPI00225318	1	1		2	3	3	2	3	1.3	2.8	0.02
IPI00270788	2	1	2	1	1	2	3	3	1.5	2.3	0.23
IPI00331322	1	1	1	1	1	1	2	2	1.0	1.5	0.13
IPI00377728	1	2						2	1.5	2.0	N/A
IPI00227235	2								2.0	N/A	N/A
IPI00122438	1			1					1.0	N/A	N/A
IPI00123276	1	3	3	1	1	2	2	2	2.0	1.8	0.70
IPI00129504	1		2					1	1.5	1.0	N/A
IPI00131366	1					1			1.0	1.0	N/A

ID	1	2	3	4	5	6	7	8			
IPI00135869	1								1.0	N/A	N/A
IPI00153702	1	1					2		1.0	2.0	N/A
IPI00169699	1		1		1				1.0	1.0	N/A
IPI00187434	1	2	1						1.3	N/A	N/A
IPI00284925	1	2	1	1	1	2			1.3	1.5	0.63
IPI00314106	1	2	1	1	2		1	1	1.3	1.3	0.85
IPI00380320	1		1	1		1	1		1.0	1.0	N/A
IPI00108194	1	1	2		1		1	1	1.3	1.0	0.37
IPI00115506	1				1		1	1	1.0	1.0	N/A
IPI00118227	1	1			2	3	1	2	1.0	2.0	0.18
IPI00133350	1	1	1	1			1	1	1.0	1.0	N/A
IPI00187405	1		1	1	1				1.0	1.0	N/A
IPI00468696	1	1							1.0	N/A	N/A
IPI00123712	2	1	1		2	2	2	3	1.3	2.3	0.07
IPI00133296	1	1	1						1.0	N/A	N/A
IPI00134131	1	2				1			1.5	1.0	N/A
IPI00230426	1	1					1	1	1.0	1.0	N/A
IPI00110918	1	2	1	1	2	1	1	2	1.3	1.5	0.54
IPI00115040	3	2		1			2	1	2.0	1.5	0.59
IPI00222753	1		1	1		2		2	1.0	2.0	N/A
IPI00224584	2	2	3	4			2	3	2.8	2.5	0.76
IPI00275992	1	1	1	2	2	2	3	1	1.3	2.0	0.17
IPI00278781	1	1	1	1	1	1	1	1	1.0	1.0	N/A
IPI00319992	1	1		1		1	1		1.0	1.0	N/A
IPI00342938	1	1			1	1			1.0	1.0	N/A
IPI00453792	1	3	1	1	5	4	2	3	1.5	3.5	0.05
IPI00462925	1					2			1.0	2.0	N/A
IPI00121280	1	1		1					1.0	N/A	N/A
IPI00229040	2	2			1		3	1	2.0	1.7	0.72
IPI00323669	1	1	1	1	1	1		1	1.0	1.0	N/A
IPI00466200	1		2		2			1	1.5	1.5	1.00
IPI00119853	1		2						1.5	N/A	N/A

ID	1	2	3	4	5	6	7	8	Avg1	Avg2	Ratio
IPI00120024	3				4				3.0	4.0	N/A
IPI00126050	1	1				1		1	1.0	1.0	N/A
IPI00331549	1								1.0	N/A	N/A
IPI00130661	1								1.0	N/A	N/A
IPI00230113	2	1		3	2	1	3		2.0	2.0	1.00
IPI00315974	1				1	2			1.0	1.5	N/A
IPI00127408	1	1	1	1	1	1			1.0	1.0	N/A
IPI00128261	1	4	2	1	1	2	1	3	2.0	1.8	0.78
IPI00229312	1								1.0	N/A	N/A
IPI00124640	1	1			1				1.0	1.0	N/A
IPI00130391	2							2	2.0	2.0	N/A
IPI00222203	1		2	3		1			2.0	1.0	N/A
IPI00132955	1				1		1		1.0	1.0	N/A
IPI00133580	1								1.0	N/A	N/A
IPI00125509	1	1		3	3		3	3	1.7	3.0	0.12
IPI00125513	2	3	2	3	2	3	2	2	2.5	2.3	0.54
IPI00229510	1		2			2	1		1.5	1.5	1.00
IPI00453724	1	1	3						1.7	N/A	N/A
IPI00928125								19	N/A	19.0	N/A
IPI00221739								2	N/A	2.0	N/A
IPI00480239								2	N/A	2.0	N/A
IPI00379169								2	N/A	2.0	N/A
IPI00378385								2	N/A	2.0	N/A
IPI00223951								2	N/A	2.0	N/A
IPI00110100								1	N/A	1.0	N/A
IPI00668724								2	N/A	2.0	N/A
IPI00308380								2	N/A	2.0	N/A
IPI00109206								1	N/A	1.0	N/A
IPI00131895								1	N/A	1.0	N/A
IPI00153640								1	N/A	1.0	N/A
IPI00911135								2	N/A	2.0	N/A
IPI00118193								1	N/A	1.0	N/A

IPI00172075			1	N/A	1.0	N/A
IPI00263048			2	N/A	2.0	N/A
IPI00515530			1	N/A	1.0	N/A
IPI00341869			3	N/A	3.0	N/A
IPI00464396			8	N/A	8.0	N/A
IPI00112377		2		N/A	2.0	N/A
IPI00127625		5		N/A	5.0	N/A
IPI00132768		3		N/A	3.0	N/A
IPI00133750		2	3	N/A	2.5	N/A
IPI00336348		3	4	N/A	3.5	N/A
IPI00387505		3		N/A	3.0	N/A
IPI00279858		9		N/A	9.0	N/A
IPI00313390		2	3	N/A	2.5	N/A
IPI00409360		4		N/A	4.0	N/A
IPI00880839		90		N/A	90.0	N/A
IPI00222125		3		N/A	3.0	N/A
IPI00344626		2		N/A	2.0	N/A
IPI00467056		3		N/A	3.0	N/A
IPI00133531		2		N/A	2.0	N/A
IPI00848508		2		N/A	2.0	N/A
IPI00466971		2		N/A	2.0	N/A
IPI00118825		90	94	N/A	92.0	N/A
IPI00116670		1		N/A	1.0	N/A
IPI00221857		1		N/A	1.0	N/A
IPI00605842		1		N/A	1.0	N/A
IPI00331318		1		N/A	1.0	N/A
IPI00111359		1		N/A	1.0	N/A
IPI00115866		1		N/A	1.0	N/A
IPI00119685		2		N/A	2.0	N/A
IPI00221564		1		N/A	1.0	N/A
IPI00165902	4	3		N/A	3.5	N/A
IPI00469542	3			N/A	3.0	N/A

IPI00131424		63		55	N/A	59.0	N/A
IPI00869393		6			N/A	6.0	N/A
IPI00889240		3			N/A	3.0	N/A
IPI00894588		174			N/A	174.0	N/A
IPI00110885		2			N/A	2.0	N/A
IPI00111255		5		3	N/A	4.0	N/A
IPI00124828		2		2	N/A	2.0	N/A
IPI00471157		2		1	N/A	1.5	N/A
IPI00311406		2			N/A	2.0	N/A
IPI00109033		2			N/A	2.0	N/A
IPI00396735		2			N/A	2.0	N/A
IPI00283755		3			N/A	3.0	N/A
IPI00378448		2			N/A	2.0	N/A
IPI00807936		2			N/A	2.0	N/A
IPI00459898		2			N/A	2.0	N/A
IPI00131548		1			N/A	1.0	N/A
IPI00136227		1			N/A	1.0	N/A
IPI00229659		2			N/A	2.0	N/A
IPI00131732		1			N/A	1.0	N/A
IPI00309964		1			N/A	1.0	N/A
IPI00605003		2		2	N/A	2.0	N/A
IPI00649765		3			N/A	3.0	N/A
IPI00132169		1			N/A	1.0	N/A
IPI00662244		2			N/A	2.0	N/A
IPI00169804	3	2	1	1	N/A	1.8	N/A
IPI00336807	3	6	4	3	N/A	4.0	N/A
IPI00110180	2				N/A	2.0	N/A
IPI00110825	4		6		N/A	5.0	N/A
IPI00226687	2				N/A	2.0	N/A
IPI00875944	2				N/A	2.0	N/A
IPI00604947	4	3	3		N/A	3.3	N/A
IPI00470086	2				N/A	2.0	N/A

IPI00671957		2	2			N/A	2.0	N/A	
IPI00120620		2				N/A	2.0	N/A	
IPI00828569		2				N/A	2.0	N/A	
IPI00112190		6			9	N/A	7.5	N/A	
IPI00648884		10				N/A	10.0	N/A	
IPI00230690		2				N/A	2.0	N/A	
IPI00667569		4				N/A	4.0	N/A	
IPI00108721		2				N/A	2.0	N/A	
IPI00133360		1				N/A	1.0	N/A	
IPI00228238		1				N/A	1.0	N/A	
IPI00874950		2				N/A	2.0	N/A	
IPI00605455		1				N/A	1.0	N/A	
IPI00406538		1				N/A	1.0	N/A	
IPI00222180		1				N/A	1.0	N/A	
IPI00222430		1				N/A	1.0	N/A	
IPI00153607		2				N/A	2.0	N/A	
IPI00173167	2						2.0	N/A	N/A
IPI00408892	2	2			2		2.0	2.0	N/A
IPI00110827	40			10			40.0	10.0	N/A
IPI00123176	2	2	2	2			2.0	2.0	N/A
IPI00222838	3						3.0	N/A	N/A
IPI00272033	4						4.0	N/A	N/A
IPI00331710	15	14					15.0	14.0	N/A
IPI00875497	52			59			52.0	59.0	N/A
IPI00453981	2	1	1	2	2		2.0	1.5	N/A
IPI00556699	3	2	3	2	3		3.0	2.5	N/A
IPI00225288	2	4	3	2	2		2.0	2.8	N/A
IPI00222447	2				2		2.0	2.0	N/A
IPI00918078	3						3.0	N/A	N/A
IPI00130118	2						2.0	N/A	N/A
IPI00221850	2						2.0	N/A	N/A
IPI00131113	2						2.0	N/A	N/A

ID	C1	C2	C3	C4	C5	C6	S1	S2	S3
IPI00229351		2					2.0	N/A	N/A
IPI00126011		1			4		1.0	4.0	N/A
IPI00515713		8					8.0	N/A	N/A
IPI00130227		1					1.0	N/A	N/A
IPI00126721		1					1.0	N/A	N/A
IPI00323406		1					1.0	N/A	N/A
IPI00111111		1					1.0	N/A	N/A
IPI00918891		3					3.0	N/A	N/A
IPI00225387		1	1				1.0	1.0	N/A
IPI00229509		1					1.0	N/A	N/A
IPI00118196		1	2			1	1.0	1.5	N/A
IPI00467181		2					2.0	N/A	N/A
IPI00356608		1					1.0	N/A	N/A
IPI00226952		1			1	2	1.0	1.5	N/A
IPI00153448		1					1.0	N/A	N/A
IPI00117832	2	2	3	2	3	2	2.0	2.5	0.31
IPI00118153	2	1			1	2	1.5	1.5	1.00
IPI00265701	3	5	2	3			4.0	2.5	0.31
IPI00331664	2						2.0	N/A	N/A
IPI00345740	3	3	6	3	4	3	3.0	4.0	0.40
IPI00604969	34	35		2	3	3	34.5	2.7	0.00
IPI00136929	17						17.0	N/A	N/A
IPI00137227	2	2	2	1	3	1	2.0	1.8	0.75
IPI00221402	3	3					3.0	N/A	N/A
IPI00355248	29	21	23	19			25.0	21.0	0.47
IPI00606510	27	27					27.0	N/A	N/A
IPI00762198	13	17			6	11	15.0	8.5	0.18
IPI00849031	3						3.0	N/A	N/A
IPI00400301	2					2	2.0	2.0	N/A
IPI00224456	2				1		2.0	1.0	N/A
IPI00330688	2	5		2	2	2	3.5	2.0	0.27
IPI00123138	2		2		2		2.0	2.0	N/A

ID								Avg1	Avg2	
IPI00123639		2						2.0	N/A	N/A
IPI00114642		2						2.0	N/A	N/A
IPI00110460		2						2.0	N/A	N/A
IPI00330225		2						2.0	N/A	N/A
IPI00109411		2						2.0	N/A	N/A
IPI00114733		1	2	1	1			1.5	1.0	0.42
IPI00118235		1						1.0	N/A	N/A
IPI00124389		1	2	1	2	1	1	1.5	1.3	0.63
IPI00128144		2			3			2.0	3.0	N/A
IPI00225751		1						1.0	N/A	N/A
IPI00315794		2	1	3		3	4	1.5	3.3	0.05
IPI00322760		1	1	1	1	1	1	1.0	1.0	N/A
IPI00377839		1						1.0	N/A	N/A
IPI00415685		1						1.0	N/A	N/A
IPI00395196		3						3.0	N/A	N/A
IPI00329913		1	1	2			1	1.0	1.5	0.42
IPI00165727		2						2.0	N/A	N/A
IPI00654317		1						1.0	N/A	N/A
IPI00759911		1						1.0	N/A	N/A
IPI00353672		2						2.0	N/A	N/A
IPI00135208		1		1				1.0	1.0	N/A
IPI00226854		1						1.0	N/A	N/A
IPI00474450		2						2.0	N/A	N/A
IPI00121319		1						1.0	N/A	N/A
IPI00110265		1	1	1	2	4	1	1.0	2.0	0.40
IPI00128209		1						1.0	N/A	N/A
IPI00894922		2						2.0	N/A	N/A
IPI00110672		1	3	3	2	2		2.0	2.3	0.72
IPI00127581		2						2.0	N/A	N/A
IPI00112227	3	3	3	3	5	2	3	3.0	3.3	0.75
IPI00119808	3		1					2.0	N/A	N/A
IPI00125939	3			2	3			3.0	2.5	N/A

ID	1	2	3	4	5	6	7	Avg1	Avg2	Ratio
IPI00153144	2	2	5	2	3	2		3.0	2.3	0.56
IPI00314919	3	2	3	5	2		3	2.7	3.3	0.52
IPI00404845	2	1				2	2	1.5	2.0	0.42
IPI00114593	14			8			16	14.0	12.0	N/A
IPI00130589	5	3	2	2	5	6	2	3.3	3.8	0.78
IPI00228497	2	2	3			3	2	2.3	2.5	0.79
IPI00283611	9							9.0	N/A	N/A
IPI00336324	2	1	2	2	2	2	2	1.7	2.0	0.29
IPI00890234	14	17				12	19	15.5	15.5	1.00
IPI00607969	2			2	2	2	2	2.0	2.0	N/A
IPI00121550	2	2	2		1	2	3	2.0	2.0	1.00
IPI00225573	2	2	1	2	2		1	1.7	1.7	1.00
IPI00118237	2			4	2	2	5	2.0	3.3	N/A
IPI00266836	2		2		2	1		2.0	1.5	0.42
IPI00109603	2						1	2.0	1.0	N/A
IPI00136655	2	2	3	2				2.3	2.0	N/A
IPI00112327	2							2.0	N/A	N/A
IPI00453801	4	2						3.0	N/A	N/A
IPI00930865	3							3.0	N/A	N/A
IPI00923106	2		1	2			1	1.5	1.5	1.00
IPI00876341	38	41					64	39.5	64.0	N/A
IPI00458039	2							2.0	N/A	N/A
IPI00408258	2							2.0	N/A	N/A
IPI00664143	2							2.0	N/A	N/A
IPI00330094	6							6.0	N/A	N/A
IPI00111884	1	1	1					1.0	N/A	N/A
IPI00120709	1	3	3		3	5	3	2.3	3.7	0.23
IPI00135132	1							1.0	N/A	N/A
IPI00319135	2	1		2	1			1.5	1.5	1.00
IPI00330272	1							1.0	N/A	N/A
IPI00648312	1					2	1	1.0	1.5	N/A
IPI00111045	1	4	3	3		3		2.7	3.0	0.79

ID	C1	C2	C3	C4	C5	C6	C7	A	B	C
IPI00138892	2	1		1	1			1.5	1.0	0.42
IPI00153842	1	1	1	2	1			1.0	1.5	0.27
IPI00170051	1			1	1	1	1	1.0	1.0	N/A
IPI00226414	1	1	1	1	1	1	1	1.0	1.0	N/A
IPI00457976	1							1.0	N/A	N/A
IPI00139788	1					1	1	1.0	1.0	N/A
IPI00229065	1					1	1	1.0	1.0	N/A
IPI00467833	1		1	1	1	2	2	1.0	1.5	0.31
IPI00471368	1	1						1.0	N/A	N/A
IPI00123186	3	1	3		3	4		2.3	3.5	0.30
IPI00221580	1	2	1	2		3	3	1.3	2.7	0.05
IPI00323748	1				2	1		1.0	1.5	N/A
IPI00133965	1	1	2	2	1	1	1	1.3	1.3	0.85
IPI00129506	1		1	1		1		1.0	1.0	N/A
IPI00110202	2							2.0	N/A	N/A
IPI00624533	2							2.0	N/A	N/A
IPI00117264	1	2				2	3	1	1.5	2.0	0.59
IPI00310827	2					2	2	2.0	2.0	N/A
IPI00115125	1							1.0	N/A	N/A
IPI00126857	1				1			1.0	1.0	N/A
IPI00126634	2	2	1	2	1	1	2	1.7	1.5	0.72

Supplementary Table 4: acetylated lysine sites of malate aspartate shuttle (MAS) proteins. K[170.11] depicts acetylation site.
N/A: no peptide identified in Control but in cKO. N/D: not determined.

Protein name	Acetylated peptide sequence	Acetylated lysine(s)	cKO/ Con	SEM	cKO+cNAMPT/ Con	% LysAc change by cNAMPT
Mitochondrial 2-oxoglutarate/malate carrier protein	M[147.04]DGK[170.11]PRTSPK	15	N/A	N/D	N/A	N/A
Mitochondrial malate dehydrogenase	GYLGPEQLPDC[160.03]LK[170.11]GC[160.03]DVVVIPAGVPR	91	7.9	4.5	0.8	-90
	M[147.04]IAEAIPELK[170.11]ASIK M[147.04]IAEAIPELKASIK[170.11]	324,328	2.2	0.8	1.2	-46
	KGLEK[170.11]NLGIGK K[170.11]GLEKNLGIGK	297,301	5.7	2.1	3.3	-42
	ANTFVAELK[170.11]GLDPAR	185	6.9	3.4	1	-85
	MIAEAIPELK[170.11]ASIK MIAEAIPELKASIK[170.11]	324,328	6.9	2.3	3.2	-53
	ITPFEEK[170.11]M[147.04]IAEAIPELK	314	5.4	1.5	1.2	-78
	IQEAGTEVVKAK[170.11] IQEAGTEVVK[170.11]AK	239,241	1.9	0.7	0.7	-62
	NLGIGK[170.11]ITPFEEK	307	4.4	1.5	2.1	-52
	HGVYNPNK[170.11]IFGVTTLDIVR	165	5.0	4.5	3	-40
	ANVK[170.11]GYLGPEQLPDC[160.03]LK	78	4.4	2.4	2.5	-43
	GLEK[170.11]NLGIGK	301	2.9	0.8	1.9	-34
	ITPFEEK[170.11]MIAEAIPELK	314	8.6	5.4	1.9	-78
	K[170.11]GEDFVK	329	4.6	2.4	1.8	-61
	KGEDFVK[170.11]NMK	335	107.2	N/D	N/A	N/A
	TIIPLISQC[160.03]TPK[170.11]VDFPQDQ LATLTGR	215	3.5	1.1	1	-71
	VNVPVIGGHAGK[170.11]TIIPLISQC[160.03]TPK	203	6.0	1.4	3.6	-40
	K[170.11]GLEK[170.11]NLGIGK	297,301	9.4	N/D	21.3	126
	ASIK[170.11]K[170.11]GEDFVK	328,329	5.6	2.8	2.9	-48

	K[170.11]HGVYNPNK	157	N/A	N/D	N/A	N/A
	EGVVEC[160.03]SFVQSK[170.11]ETEC[160.03]TYFSTPLLLGK	281	1.6	0.7	0.3	**-82**
	ETEC[160.03]TYFSTPLLLGK[170.11]K ETEC[160.03]TYFSTPLLLGKK[170.11]	296,297	5.2	2.3	2	**-62**
	KGEDFVK[170.11]NM[147.04]K	335	N/A	N/D	N/A	N/A
	GLEK[170.11]NLGIGK[170.11]ITPFEEK	301,307	5.2	N/D	5.1	**-1**
	GEDFVK[170.11]NM[147.04]K	335	N/A	N/D	N/A	N/A
Mitochondrial aspartate aminotransferase	VGAFTVVC[160.03]K[170.11]DAEEAKR VGAFTVVC[160.03]KDAEEAK[170.11]R	296,302	6.3	1.8	1.6	**-75**
	AEAQIAAK[170.11]NLDKEYLPIGGLAEFC[160.03]K AEAQIAAKNLDK[170.11]EYLPIGGLAEFC[160.03]K	90,94	4.1	1.5	N/A	N/A
	DVFLPK[170.11]PSWGNHTPIFR	159	49.7	N/D	2.0	**-96**
	EFSVYMTK[170.11]DGR	404	3.3	1.9	3	**-9**
	EGSSHNWQHITDQIGMFC[160.03]FTGLK[170.11]PEQVER	387	14.6	N/D	2.7	**-81**
	YYDPK[170.11]TC[160.03]GFDFSGALEDISK	185	11.9	6.3	3.1	**-74**
	DDNGK[170.11]PYVLPSVR	73	3.5	1.6	1.6	**-55**
	AEAQIAAK[170.11]NLDK AEAQIAAKNLDK[170.11]	90,94	1.8	0.7	1.7	**-4**
	QWLQEVK[170.11]GMADR	345	7.4	3.7	5	**-32**
	VGAFTVVC[160.03]K[170.11]DAEEAK	296	4.8	2.8	1.9	**-61**
	QWLQEVK[170.11]GM[147.04]ADR	345	1.9	1.1	1.3	**-33**
	IPEQSVLLLHAC[160.03]AHNPTGVDPRPEQWK[170.11]EIASVVK	227	N/A	N/D	N/A	N/A
	LTK[170.11]EFSVYM[147.04]TK	396	3.4	1	0.9	**-74**
	TQLVSNLK[170.11]K	363	2.9	1.1	1.7	**-42**

	Peptide	Residue				
	K[170.11]AEAQIAAK[170.11]NLDK K[170.11]AEAQIAAKNLDK[170.11]	82,90,94	2.3	1.1	1.1	**-52**
	NLDKEYLPIGGLAEFC[160.03]K[170.11]A SAELALGENNEVLK	107	N/A	N/D	N/A	N/A
	NLDK[170.11]EYLPIGGLAEFC[160.03]K	94	1.3	0.7	0.7	**-46**
	VESQLK[170.11]ILIRPLYSNPPLNGAR	309	N/A	N/D	N/A	N/A
	LTK[170.11]EFSVYMTK	396	4.1	1.7	5.7	**38**
	FFK[170.11]FSR	150	21.0	18.3	4.1	**-81**
	VGAFTVVC[160.03]K[170.11]DAEEAK[170 .11]R	296,302	N/A	N/D	N/A	N/A
	ASAELALGENNEVLK[170.11]SGR	122	3.8	1.2	3.3	**-13**
	KAEAQIAAK[170.11]NLDK	90	3.5	1.3	2.4	**-32**
Mitochondrial aspartate glutamate carrier 1	EEGPSAFWK[170.11]GTAAR	578	1.0	0.6	1.6	**57**
Mitochondrial aspartate glutamate carrier 2	ALWK[170.11]GVAAR	581	4.6	2	2	**-56**
	DLGFFGIYK[170.11]GAK	485	N/A	N/D	N/A	N/A

Supplementary Table 5: acetylated lysine sites of proteins linked to mPTP. K[170.11] depicts acetylation site. N/A: no peptide identified in Control but in cKO. N/D: not determined.

Protein name	Acetylated peptide sequence	Acetylated lysine(s)	cKO/ Con	SEM	cKO+cNAMPT/ Con	% LysAc change by cNAMPT
Cyclophilin D	ALC[160.03]TGEK[170.11]GFGYK	85	1.9	0.6	1.2	**-37**
	VVLELK[170.11]ADVVPK	66	1.9	0.6	0.9	**-53**
	ADVVPK[170.11]TAENFR	72	1.7	0.8	1.4	**-16**
Oligomycin sensitivity conferral protein	TVLK[170.11]SFLSPNQILK	162	3.6	1.6	2.3	**-37**
	SFLSPNQILK[170.11]LEIK[170.11]	172 or 176	5.1	2.8	1.6	**-69**
	YATALYSAASK[170.11]EK[170.11]	51 or 53	3.3	2.5	1	**-70**
	LDQVEK[170.11]ELLR	60	3.4	1.7	1.9	**-43**
	EK[170.11]FSPLTANLMNLLAENGR	100	N/A	N/D	N/A	N/A
	VGQLLK[170.11]DPK	70	2.6	1	1.1	**-58**
	K[170.11]LDQVEK[170.11]ELLR	54 or 60	N/A	N/D	N/A	N/A
	IGEK[170.11]YVDMSAK	192	2.5	1.3	2.6	**4**
	VK[170.11]SLNDITK	90	1.1	0.3	0.7	**-39**
Voltage-dependent anion-selective channel protein 1	GYGFGLIK[170.11]LDLK	41	30.5	6.7	7.5	**-75**
	LTLSALLDGK[170.11]NVNAGGHK	279	2.0	0.5	1.6	**-19**
	YQVDPDAC[160.03]FSAK[170.11]VNNSS LIGLGYTQTLKPGIK	249	N/A	N/D	N/A	N/A
	FGIAAK[170.11]YQVDPDAC[160.03]FSAK	237	3.2	1.9	1.3	**-60**
	VNNSSLIGLGYTQTLK[170.11]PGIK	265	3.9	2.8	1.7	**-56**
	DVFTK[170.11]GYGFGLIK	33	2.7	0.9	1.6	**-41**
	VNGSLETK[170.11]YR	74	1.2	0.5	0.4	**-67**
Voltage-dependent anion-selective channel protein 2	DIFNK[170.11]GFGFGLVK	32	2.7	0.9	1.2	**-55**
	GFGFGLVK[170.11]LDVK	40	N/A	N/D	N/A	N/A
	YK[170.11]WC[160.03]EYGLTFTEK	75	1.5	0.6	1.0	**-32**
	VSGTLETK[170.11]YK VSGTLETKYK[170.11]	73,75	1.0	0.8	3.5	**248**
Voltage-dependent	YK[170.11]VC[160.03]NYGLTFTQK	63	3.7	1.2	2.0	**-46**

anion-selective channel protein 3	AAK[170.11]DVFNK	15	3.4	1.8	1.4	**-59**
	YK[170.11]LDC[160.03]R	226	1.5	0.8	1.3	**-15**
	ASGNLETK[170.11]YK	61	0.8	N/D	0.2	**-73**
	LSQNNFALGYK[170.11]AADFQLHTHVND GTEFGGSIYQK	174	N/A	N/D	N/A	N/A
	DVFNK[170.11]GYGFGM[147.04]VK	20	N/A	N/D	N/A	N/A
	GYGFGM[147.04]VK[170.11]IDLK	28	1.5	N/D	0.0	**-100**
ADP/ATP translocase 1	IAK[170.11]DEGANAFFK	263	3.7	1.1	1.4	**-62**
	DEGANAFFK[170.11]GAWSNVLR	272	2.5	0.6	6.5	**158**
	YFPTQALNFAFK[170.11]DK YFPTQALNFAFKDK[170.11]	92,94	5.3	1.9	3.4	**-36**
	DFLAGGIAAAVSK[170.11]TAVAPIER	23	6.9	2.9	2.6	**-62**
	YK[170.11]QIFLGGVDR	96	2.5	N/D	1.9	**-25**
	IFK[170.11]SDGLK	166	1.4	0.9	0.6	**-56**
	AAYFGVYDTAK[170.11]GMLPDPK	199	N/A	N/D	N/A	N/A
	IPK[170.11]EQGFLSFWR	63	N/A	N/D	N/A	N/A
	EFNGLGDC[160.03]LTK[170.11]IFK	163	0.6	0.4	0.5	**-16**
	LAADVGK[170.11]GSSQR	147	N/A	N/D	N/A	N/A
ADP/ATP translocase 2	GLGDC[160.03]LVK[170.11]IYK	163	0.4	N/D	9.2	**2442**
	DFLAGGVAAAISK[170.11]TAVAPIER	23	5.0	2.7	1.2	**-76**
	EFK[170.11]GLGDC[160.03]LVK	155	N/A	N/D	N/A	N/A